TÉCNICO LISBOA

Experimental study of a venturi ejector for passive recirculation of hydrogen in PEM fuel cell systems

Pedro Miguel Henriques Pires da Silva Rodrigues

Thesis to obtain the Master of Science Degree in

Energy Engineering and Management

Supervisors: Dr. Rui Pedro da Costa Neto
Eng. Jos Lenssen

Examination Committee

Chairperson: Prof. Edgar Caetano Fernandes
Supervisor: Dr. Rui Pedro da Costa Neto
Member of the Committee: Dr. Daniela Sofia de Castro Falcão

July 2022

Declaração

Declaro que o presente documento é um trabalho original da minha autoria e que cumpre todos os requisitos do Código de Conduta e Boas Práticas da Universidade de Lisboa.

Declaration

I declare that this document is an original work of my own authorship and that it fulfills all the requirements of the Code of Conduct and Good Practices of the Universidade de Lisboa.

To my mother.

”Ik ben op zoek, ik streef, ik zit erin met heel mijn hart.“

Vincent van Gogh

Acknowledgments

This thesis marks the much anticipated end of a cycle in Instituto Superior Técnico. A cycle where I met colleagues that became family, professors that became friends, and engineers that became mentors.

I would like to thank Dr. Rui Pedro da Costa Neto for opening his door to me three years ago when I was committed to building a fuel cell powered vessel, even more so when he was kind enough to accept a theme for this thesis proposed by me. It could have gone wrong, but fortunately, due to engineer Jos Lenssen from Nedstack Fuel Cell Technology BV, it didn't. Thank you, Jos, for allowing me into the company and providing me with all the necessary equipment and funding to pursue this work in the Netherlands. For their companionship in the office, thank you Ali Saadabadi, Danilo Damiano, and Mark Lameris. In particular, thank you, Mark, for all your patience and guidance.

For providing me with my career path, I must acknowledge Técnico Solar Boat. There is and always will be a before and after TSB. By the slightest chance, I ended up being in the right place and right time to make history in the journey of this project and our country. I was challenged like never before during my time in the project, both technically and humanly, and managed to rise above the difficulties accompanied by my teammates to bring to life São Miguel 01: a PEM fuel cell prototype vessel, the first of its kind ever built in Portugal and whose name honors one of the vessels that set sail in Vasco da Gama's armada to discover the sea route to India in the late XV century. We, too, are finding new routes in the maritime sector, just like before.

Finally, the most important acknowledgements go to my loved ones, who always provided me with the necessary support and who many times believed in me before I believed in myself.

Resumo - [PT]

Este estudo pretende explorar uma oportunidade de aumentar a efficiência de sistemas com células de combustível PEM substituindo a bomba de recirculação de hidrogénio por uma solução passiva, um ejetor de venturi.

Uma abordagem experimental foi implementada onde múltiplos factores que caracterizam as condições de funcionamento de uma célula de combustível foram estudados. Nomeadamente, foram obtidas curvas I-V, caudais de consumo de hidrogénio e ar, as quedas de pressão no ânodo e no cátodo foram registadas, assim como as temperaturas e humidades relativas. Estas variáveis foram obtidas para um sistema com ânodo aberto, com uma bomba de recirculação e com um ejetor de venturi.

Os resultados deste estudo validam parcialmente a utilização do ejetor de venturi estudado. O estudo mostra que os sistemas têm curvas I-V estáveis, perfis de consumo de hidrogénio e ar e quedas de pressão no ânodo semelhantes. No entanto, o caudal de recirculação imposto pelo ejetor de venturi revelou-se insuficiente para manter uma humidade relativa no ânodo acima de 40%, à temperatura da stack, 65℃. Finalmente, a utilização do ejetor para recirculação de hidrogénio resulta numa poupança de 60% do consumo de energia quando comparado com a utilização da bomba.

Palavras-chave: Células de combustível, Recirculação ativa de hidrogénio, Recirculação passiva, Ejetor de venturi

Samenvatting - [NL]

Deze studie verken de mogelijkheid om de efficiëntie van een PEMFC systeem te vergroten. Met name de mogelijkheid om een energievraagingpomp voor waterstofrecirculatie in de anode van een PEMFC met een venturi-ejector, een passief apparat.
Er werd een experimentele benadering van dit onderwerp gevolgd waarbij meerdere factoren die de werkomgeving van een PEMFC werden bestudeerd. Er werden namelijk IV-curven verkregen, waterstof en luchtstroom snelheden werden gemeten, de drukval in de anode werd geregistreerd, evenals de inlaattemperatuur en relatieve vochtigheid. Deze variabelen werden verkregen voor een systeemopstelling in open anode, die een membraanpomp en een venturi-ejector.
De resultaten van deze studie valideren gedeeltelijk het gebruik van de venturi-ejector. De studie toonde aan: dat de systemen een vergelijkbare en stabiele IV-curve, waterstof- en luchtstroomverbruiksprofielen bieden en anode- en kathodedruk daalt. Niettemin is het recirculatiedebiet opgelegd door de venturi ejector lijkt onvoldoende te zijn om een aanbevolen relatieve vochtigheid van de anode boven 40% te houden op de stapel temperatuur, 65℃. Ten slotte resulteert het gebruik van de venturi-ejector voor waterstofrecirculatie in een 60% afname van de energievraag in vergelijking met het gebruik van de pomp.

Keywords: PEM fuel cell , Active recirculation, Passive recirculation, Venturi ejector

Abstract - [EN]

This study explores an opportunity to increase a PEM fuel cell system efficiency by replacing an energy-demanding pump with a passive device, a venturi ejector, to perform hydrogen recirculation in the fuel cell's anode.

An experimental approach to this subject was taken where multiple factors that characterize the working environment of a PEMFC were studied. Namely, I-V curves were obtained, hydrogen and air flow rates were measured, the pressure drop in the anode was recorded, as well as the inlet temperature and relative humidity. These variables were obtained for a system set-up in open anode, encompassing a diaphragm pump and a venturi ejector.

The results of this study partially validate the utilization of the venturi ejector. The study showed that the systems provide similar and stable I-V curves, hydrogen and air flow consumption profiles, and anode and cathode pressure drops. Nevertheless, the recirculation flow rate imposed by the venturi ejector seems insufficient to keep a recommended anode relative humidity above 40%, at stack temperature, 65℃. Finally, the utilization of the venturi ejector for hydrogen recirculation results in a 60% energy saving compared to the utilization of the pump.

Keywords: PEM fuel cell, Active recirculation, Passive recirculation, Venturi ejector

Contents

List of Tables

List of Figures

Nomenclature

Acronyms

BOL	Begining Of Life.
BOP	Balance Of Plant.
CAN	Controller Area Network.
DQC	Detailed Quality Control.
EOL	End Of Life.
EU	European Union.
FC	Fuel Cell.
FM	Flow Meter.
GDL	Gas Diffusion Layer.
HOR	Hydrogen Oxidation Reaction.
MEA	Membrane Electrode Assembly.
OA	Open Anode.
ORR	Oxygen Reduction Reaction.
PEM	Proton Exchange Membrane.
PEMFC	Proton Exchange Membrane Fuel Cell.
RH	Relative Humidity.
USD	United States Dollar.
WMO	World Meteorological Organisation.

Greek symbols

Δ	Absolute deviation.
δ	Relative deviation.

Ω cross sectional.

Φ Recirculation ratio.

ρ density.

Roman symbols

ΔV_a Activation polarization drop.

c Velocity.

m Concentration loss coefficient.

P Pressure.

p Pressure.

R Ideal gas constant.

ΔG^0 Change in Gibbs free energy.

ΔV_Ω Ohmic drop.

ΔV_c Concentration polarization drop.

A Activation loss coefficient.

h Enthalpy.

i Current density.

I Current.

L_c Length of the unit cell.

L_m Membrane thickness.

m Mass flow rate.

N Anode nitrogen flow.

n Concentration loss exponent.

P_N Nitrogen partial pressure.

P_r Partial pressure of non-vapor gases.

Q_R Reaction quotient.

R_Ω Specific resistance.

T Temperature.

V_{fc} Voltage of the fuel cell.

W Width of the unit cell.

F Faraday's constant.

V_r^0 Electrochemical cell open circuit reversible voltage.

$\dot{V}$ Volumetric flow rate.

Chapter 1

Introduction

1.1 Motivation

The World Meteorological Organisation (WMO) reported that 2020 was one of the three warmest years on record [1], Figure 1.1. The Paris Agreement defines in Article 2 - 1 (a) that the global average temperature raise to be held to 2 ℃ and preferably to 1.5 ℃ above pre-industrial levels [2]. The European Union (EU) and its Member States, acting jointly, are committed to a binding target of a net domestic reduction of at least 55% in greenhouse gas emissions by 2030 compared to 1990 [3]. Hydrogen ($\mathrm{H_2}$), as a key energy transition pillar, is gathering a strong momentum with over 30 countries having released hydrogen road maps, more than 200 hydrogen projects announced by the industry, over USD 70 billion in public funding and an additional investment of USD 300 billion from the private sector. Moreover, Hydrogen Council now represents a 6.6 trillion market capitalization with more than 6.5 million employees globally [4, 5]. Portugal and The Netherlands, where the present work was conducted, aim to have installed 4 GW and 2 GW of electrolyser capacity by 2030, respectively, for green hydrogen production [6–8].

In the effort to contribute to these goals this work tackles a very small part of the solution. Hydrogen recirculation in PEMFCs is a key factor in the efficiency of the energy generation process [9–11]. Current hydrogen recirculation processes are in its majority addressed via active recirculation, meaning, with the usage of a pump, increasing energy consumption and consequently decreasing efficiency [12, 13]. Passive recirculation using a venturi ejector is a potential alternative [14, 15]. The fact that its operation is strictly mechanical and so, no electricity required for operation, there is the potential to furthermore increase the efficiency of energy generation in PEMFCs [16]. A venturi ejector converts potential energy from the high-pressure hydrogen tank into kinetic energy and the increased flow velocity through a tapered nozzle forms a vacuum area at the exit of the nozzle dragging the recirculated flow [17]. The entrainment flow is then a mixture of dry hydrogen ($\mathrm{H_2}$) and high relative humidity (RH%) hydrogen that has the required properties for anode inlet in PEMFCs [18].

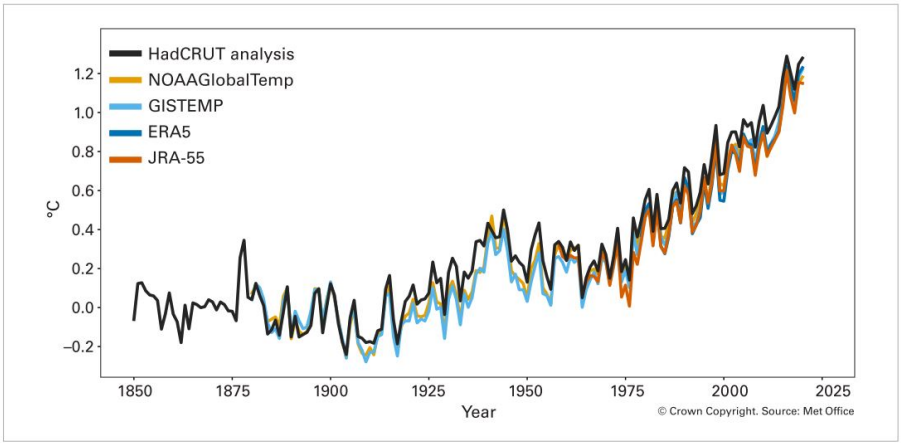

Figure 1.1: Global annual mean temperature difference from pre-industrial conditions (1850–1900) for five global temperature data sets [1].

1.2 PEMFC

Proton Exchange Membrane Fuel Cells (PEMFCs) have been used as a primary power source in transportation and stationary applications for more than 20 years [13, 19, 20]. PEMFCs have pollution free emissions and its materials are more than 80% recyclable [21–23]. A PEMFC encompasses two electrodes and an electrolyte, Figure 1.2. A redox reaction is the basis of its operation. The oxygen reduction reaction (ORR) takes place on the cathode side and the hydrogen oxidation reaction (HOR) occurs on the anode side. Between the cathode and anode catalyst layers, typically composed by carbon and platinum, a Proton Exchange Membrane (PEM), also known as a Proton Electrolyte Membrane (PEM), acts as the electrolyte allowing the flow of ionic charge [24]. This membrane only allows the hydrogen protons, H^{+}, to pass through, whereas the electrons, e^{-}, are collected and utilized as electricity [25]. A Gas Diffusion Layer (GDL) on both sides of the assembly composed by the PEM and catalyst layers absorbs the hydrogen and the oxygen on the anode and cathode sides, respectively, acting as an electrode and allowing the diffusion of the gases along the membranes, helping to remove water at the same time. A Membrane Electrode Assembly (MEA) is the assembly of the PEM membrane with the catalyst layers and GDLs. The equations that describe the reactions taking place in a PEMFC are shown in Figure 1.2.

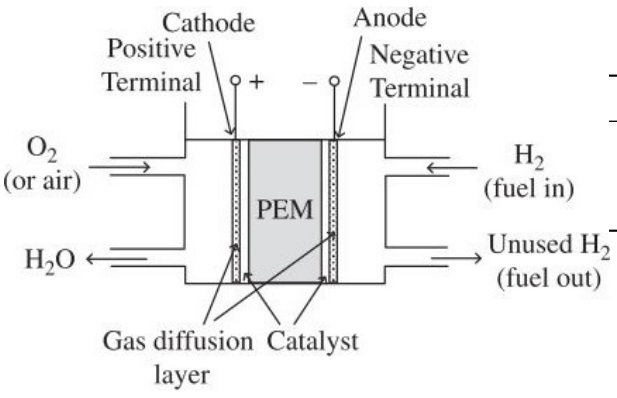

Electrode	Reaction	Equation
Cathode	Reduction	$O_2 + 4H^+ + 4e^- \rightarrow 2H_2O$
Anode	Oxidation	$2H_2 \rightarrow 4H^+ + 4e^-$
Cell		$2H_2 + O_2 \rightarrow 2H_2O$

Figure 1.2: PEMFC structure and basic reaction equations [24].

The voltage of a PEMFC is in the range of 0.5 V to 1 V, so PEMFCs are arranged in stacks of hundreds of cells in series and the latter in parallel to increase power capability [24]. A PEMFC can be described by an electrochemical model for open circuit. An electrochemical cell open circuit reversible voltage, V_r^0, is related to the change in Gibbs free energy, ΔG^0, by Equation 1.1

$$V_r^0 = -\frac{\Delta G^0}{2F}. \tag{1.1}$$

where F is the Faraday's constant (96.485 J/Vmol) and 2 is the number of moles of electrons according to the balanced equation for the redox reaction [24]. The voltage of the fuel cell can also include the effects of the reaction quotient as described by the Nernst Equation 1.2

$$V_{fc} = V_r^0 - \frac{RT}{2F} log_e Q_R. \tag{1.2}$$

where R is the ideal gas constant (8.314 J/mol K) , T is the temperature and Q_R is the reaction quotient. The cell voltage, being dependent on the cell current is also dependent on the number of voltage drops within the cell. The three important voltage drops are ohmic, activation and concentration. The ohmic drop, ΔV_Ω, is the summation of ohmic drops due to terminations and current collectors and can be described by Equation 1.3.

$$\Delta V_\Omega = R_\Omega i_{fc}. \tag{1.3}$$

where R_Ω is the PEMFC specific resistance (Ωm^2) and i_{fc} is the current density (A/m^2). The activation polarization drop, ΔV_a, is due to charge transfer reactions faced by the electrons at the electrode-electrolyte junctions and can be described by Equation 1.4, also known as the Tafel equation, named after the Swiss chemist Julian Tafel (1862 - 1918) [24].

$$\Delta V_a = A log_e(\frac{i_{fc}}{i_0}), i_{fc} \geq i_0. \tag{1.4}$$

where, i_0 is the current density and A the activation loss coefficient. The relevance of this drop decreases from low power to full power operation. The concentration polarization drop, ΔV_c, is the internal resistance faced by the ions due to the electrolyte concentration and can be described by Equation 1.5.

$$\Delta V_c = m e^{n i_{fc}}. \tag{1.5}$$

where m is the concentration loss coefficient and n the concentration loss exponent. Thus, the PEMFC voltage given by Equation 1.2 can be rearranged into Equation 1.6 to include the voltage drops above.

$$V_{fc} = V_r^0 - \Delta V_\Omega - \Delta V_a - \Delta V_c. \tag{1.6}$$

These voltage drops can also be observed in the typical polarization curve of a PEMFC. The polarization curve characterizes a PEMFC and represents the plot of its voltage as a function of the specific current, Figure 1.3.

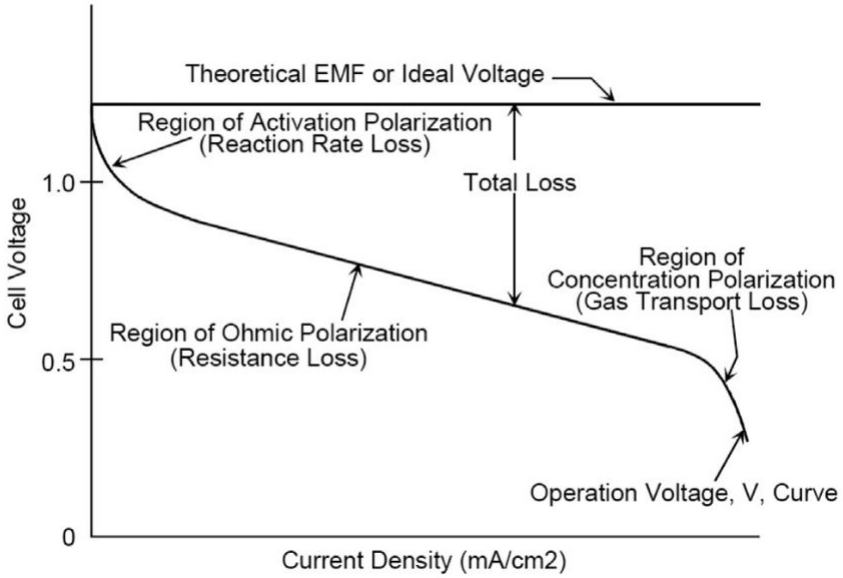

Figure 1.3: Typical polarization curve of a PEMFC [26].

1.3 Hydrogen recirculation

To ensure a good performance and durability of a PEMFC, hydrogen, H_2, is supplied to the stack in excess, resulting in a stoichiometry greater than one [27]. This is so to prevent hydrogen starvation in the MEA [28, 29]. Hydrogen continuously flows through the anode and only a portion of the gas is consumed. This implies that a substantial amount of hydrogen is present in the exhaust gas from the anode. The general treatment of the unused humidified hydrogen in the stack anode is to recirculate it back to the anode ensuring a good humidification of the MEA required for the good operation and longevity of the PEMFC. The recirculation of the anode exhaust humidified hydrogen originates two main issues such as nitrogen, N_2, crossover and flooding.

With MEAs growing thinner in recent years, understanding gases permeability through the membrane is increasingly important [30, 31]. Present in air, nitrogen, N_2, crosses the MEA from the cathode to anode side diluting the hydrogen, H_2. This increases anode polarization resulting in lower cell performance. Moreover, nitrogen, N_2, accumulation at certain spots causes localized fuel starvation, leading to cathode catalyst support corrosion and inducing catalyst degradation [31]. A typical solution is to include a bleed valve to periodically purge the system. Nitrogen, N_2, crossover can be described in steady state by Equation 1.7 [32], where N is the anode nitrogen flow $(mols^{-1})$, P_r the partial pressure of non-vapor gases (Pa), P_N is the nitrogen partial pressure (Pa), L_m is the membrane thickness (m), W is the width of the unit cell (m), L_c is the length of the unit cell (m), T is the temperature (K) and i is the current density (A/cm^2).

$$\frac{dN}{dy} = \frac{K_N}{L_m RT} W P_N \left[1 - \frac{P_r}{P_N} \frac{N}{N + (sL_C - y)(\frac{iW}{2F})}\right]. \tag{1.7}$$

In order to have high enough proton conductivity, MEAs require humidification. Water is formed on the cathode due to the proton combined ORR and not on the anode. Nevertheless, some water molecules

are transported through the membrane to the anode side due to back diffusion effect. On the anode side, the protons resultant from the HOR cross the MEA accompanied by water molecules due to electroosmotic effect. When the amount of back diffusion water is greater than that of electroosmotic water, anode flooding is highly probable to occur. Anode flooding will prevent fuel transport to electrocatalysts and thus induce high anode polarization and possible fuel starvation [32, 33].
Finally, the mainstream procedure in the industry is to use an electrical pump to perform recirculation of humidified hydrogen [34, 35]. This pump will use the electrical power generated by the PEMFC decreasing the overall efficiency of a system. Therefore, an ongoing challenge is to come up with an efficient method of reintroducing unused humidified hydrogen back into the main hydrogen supply. An alternative option that has been widely studied in literature in recent years is to adopt the use of a venturi ejector [36].

1.4 Venturi ejector

A typical venturi ejector is composed by a suction chamber, a mixing chamber and a diffusor as depicted in Figure 1.4. It uses the potential energy of the pressurized primary fluid to pump the secondary fluid by accelerating the primary fluid through the nozzle of the ejector, thus decreasing its pressure and approaching either subsonic or supersonic flow rate while generating a shock wave. Both flows mix in the mixing chamber until an homogeneous mixture is reached. Finally, a diffusor reduces the flow rate and increases the static pressure.

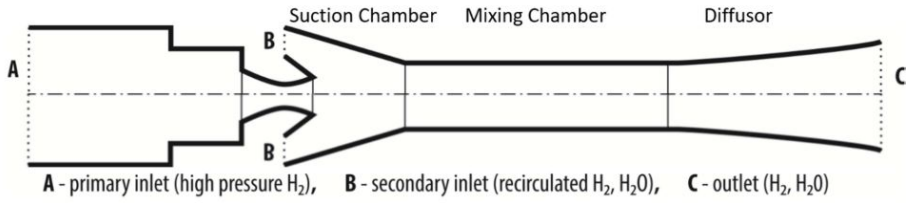

Figure 1.4: Structure scheme of a typical ejector [32]

A key parameter for measuring the ejector performance is the entrainment ratio which is the mass ratio between the secondary and primary fluid. This ratio is influenced by the geometrical parameters of the venturi ejector such as the nozzle divergent part length, nozzle diameter, nozzle exit position, mixing chamber length, mixing chamber diameter, diffusor length, diffusor angle and the chamfering fillet in the chambers. Ideally, the nozzle is designed so that the secondary flow is adequately accelerated by the primary flow and keeps friction and kinetic energy losses as small as possible. The ratio between the mixing chamber length and diameter also impacts the entrainment ratio. A preliminary geometry can be obtained from a simplified design model composed by the continuity Equation 1.8, the momentum Equation 1.9 and the energy Equation 1.10 where m is the mass flow rate (kg/s), ρ is the density (kg/m^3) of the fluid, Ω the cross sectional area (m^2) of inlet/outlet , p is the pressure (Pa), c is the velocity (m/s) and h is the enthalpy (J/kgK).

$$m_1 + m_2 = \rho_3 c_3 \Omega_3. \tag{1.8}$$

$$\rho_3 \Omega_3 - \rho_1 \Omega_1 - p_2 \Omega_2 - \int_{1-2}^{3} p d\Omega = m_1 c_1 + m_2 c_2 - m_3 c_3. \tag{1.9}$$

$$m_1(h_1 + \frac{c_1}{2}) + m_2(h_2 + \frac{c_2}{2}) = m_3(h_3 + \frac{c_3}{2}). \tag{1.10}$$

Relevant parameters affecting the entrainment ratio of an ejector are the primary, secondary and back-flow pressures being the primary flow pressure the one that will actually regulate the flow. Accordingly, the ejector performance can be divided into three operational modes: back flow, subcritical and critical. The primary flow increases with primary pressure increase whereas the secondary flow behaviour differs in each mode of operation. In back flow, the primary pressure is too low not allowing the necessary entrainment. In subcritical mode the ejector starts entraining with increased primary pressure and flow, setting a pressure of entrainment P_E. The critical mode is defined for a critical pressure, P_C, when shock waves start to appear. These pressures and operational modes are schematically depicted in Figure 1.5 [32, 37].

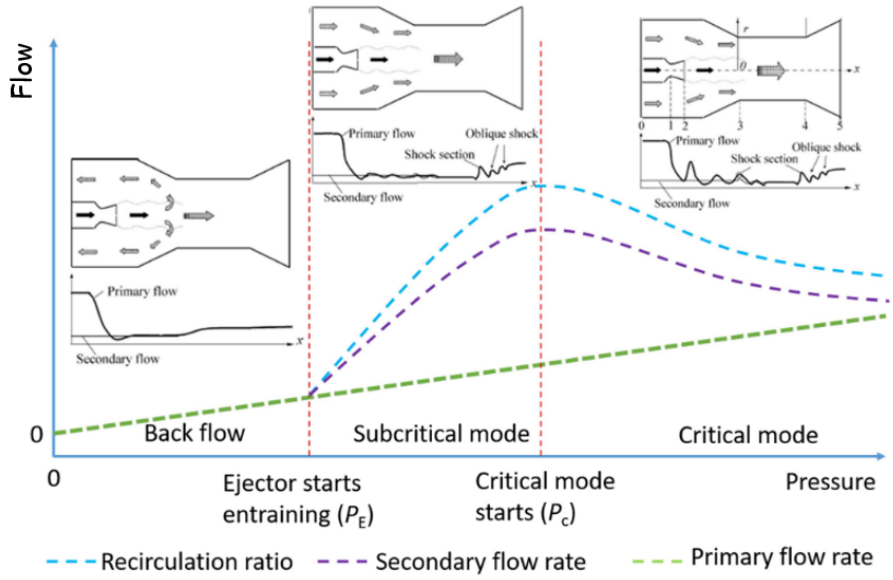

Figure 1.5: Schematic ejector performance under different operation modes, adapted from [32].

1.5 State of the art

The literature has seen an increasing number of studies in recent years concerning the use of a venturi ejector in PEMFC systems. However, the first link between a venturi ejector and PEMFC was established in 2003 when McCurdy *et al.* [38] applied one to oxygen recycling in space power applications [10]. Recently, most studies address the influence of ejector geometry in different factors or simply study the performance of an ejector in different operating conditions. However, there are few studies that compare the performance of an ejector against an active pump, in particular, an experimental comparison of both mechanisms could not be found. Huang *et al.* [39] created a model of a recirculation system where they compared the total efficiency of the system with active and passive recirculation. The latter registered a higher efficiency, as expected. Moreover, they proved that the recirculation mechanisms are influenced by the pressure at hydrogen outlet concluding that higher pressure means higher recovery rate. The efficiency of the system could also be increased by increasing the temperature of the hydrogen supply in constant flow. Toghyani *et al.* [27] developed a thermodynamic model for an ejector and an electrochemical pump. They verified that increasing the working temperature increases the performance of both the ejector and the electrochemical pump, that the recirculation ratio and hydrogen stoichiometric of the ejector increase at higher operating point and that the increase of hydrogen RH% leads to an increase of the secondary mass flow rate of the ejector leading to higher recirculation ratio. Table 1.1 summarizes the most relevant work that contributed to this study.

1.6 Scope of the work

The present work has the main objective of analysing the use of a venturi ejector for passive recirculation of hydrogen in PEMFC systems being this the first experimental approach of Nedstack fuel cell technology B.V. to the topic. A 5.5kW PEMFC is used for this study. In order to try to validate the use of the venturi ejector, a characterization of the behaviour of the relative humidity difference, $\Delta HR\%$, temperature difference, ΔT, pressure difference, ΔP, between the inlet and outlet of the anode side, and of the dry hydrogen consumption, $\dot{V}$, induced by the venturi ejector is performed and compared to a recirculation pump and open-anode scenario. The study is performed for the maximum allowed capacity of the test station used, corresponding to 0-160 A. In that range I-V curves are extracted and start-up/shut-down and ramp-up/ramp-down procedures are executed. From the main objective, specific questions were delineated:

1. How does the $\Delta HR\%$, ΔT, ΔP and $\dot{V}$ on the anode side compare in open anode, active and passive recirculation during an I-V curve test?

2. How does the ejector respond to start-up: 0 A to 40 A/shut-down: 40 A to 0 A and ram-up: 40A to 120A/ramp-down: 120A to 40A procedures?

3. What is the system's efficiency increase when using the venturi ejector alternatively to the recirculation pump?

Additional questions raised during the experimental work that were not possible to tackle during the lifetime of this study were remitted as guidelines for future work. Finally, based on previous research found in the literature, the use of the venturi ejector is expected to be validated. More scenarios must, yet, be studied to obtain a fully validated, production-ready, alternative.

1.7 Outline

This thesis is organized in five chapters. Chapter 1 provides an overview of the efforts taking place to tackle climate change, in particular, where it regards to hydrogen use. A brief explanation of PEMFCs and the importance of hydrogen recirculation is conducted. Chapter 2 explains the experimental setup and equipment used in the laboratory. The performance curves of the ejector and the PEMFC are presented in Chapter 3. Chapter 4 presents and analyses the experimental results obtained. Finally, Chapter 5 summarizes the most important conclusions and presents guidelines for future work.

Table 1.1: Venturi ejectors in the literature.

Year	Analysis	Method		Influence factors	Influenced factors	Conclusions	Ref.
		Numerical	Experimental				
2021	Recirculation rates of active and passive recirculation	Matlab/Simulink	-	Active and passive recirculation, dead-end, current density	Stack's power, voltage, temperature and efficiency, primary flow, recirculation ratio	The ejector leads to lower energy consumption. Greater the pressure, greater the recirculation ratio.	[39]
2021	PEMFC performance degradation with dual ejector	-	Test Station	MEAs material and current density	Current, impedance, voltage	The ejector adapts to changing flows. Recirculation increases performance of the FC.	[9]
2021	Ejector performance analysis	ANSYS Fluent	Bespoke setup	Stack's power and temperature, secondary flow humidity	Back pressure, entrainment and recirculation ratio	The ejector is significantly influenced by the relative humidity and temperature.	[10]
2021	Twin-nozzle ejector	Gambit and ANSYS Fluent	Bespoke setup	Power, primary and outlet pressure	Primary flow and pressure, recirculation ratio	The two-nozzle ejector presents a more symmetrical flow field. Recirculation decreases with increased back-pressure.	[23]
2020	Hydrogen supply stability and I-V curve performance	COMSOL and Matlab/Simulink	-	Primary pressure	In and outlet flows, temperature, pressure and velocity distributions	Increasing the ejector's inlet pressure increases the outlet flow and decreases it's temperature, harming the removal of humidity.	[40]
2020	Ejector transient characteristics	OpenFOAM	-	Primary pressure, nitrogen-hydrogen ratio in secondary flow, power, geometric	In and outlet flows , entrainment ratio, outlet humidity	The hydrogen supply can be controlled by the ejector primary flow pressure. The inlet relative humidity of the secondary flow should be maintained less than 85% at 353K.	[36]
2019	Compressor vs. ejector vs. electrochemical pump	Analytical	-	Active area, current density, number of cells, primary pressure, anode relative humidity and temperature	Efficiency, pump power, stoichiometric ratio, recirculation ratio, voltage	The recirculation ratio increases with temperature.	[27]
2019	Ejector for a 80 kW PEMFC	ANSYS Fluent	Bespoke setup	Power, primary and outlet pressure	Primary flow, entrainment ratio, anode pressure	Humidity significantly influences recirculation.	[14]
2018	Power ramp rate capabilities	Matlab/Simulink	Test Station	Primary flow	Stack's current, voltage and power, cooling temperature, primary pressure	Stack can be ramped-up from 2.0kW to 4.0kW in 0.1s.	[11]
2018	Hybrid system	ANSYS Fluent	Bespoke setup	Primary and secondary pressure, secondary temperature	Sensitivity analysis	The ejector model was successfully validated against experimental data.	[17]
2017	Variable-geometry ejector with a two stage cascaded stack	ANSYS Fluent	Test Station	Current, hydrogen stoichiometry	Diameter of mixing tube, primary flow, anode pressure, voltage	The number of stages decreases the global hydrogen excess ratio.	[41]
2017	Water vapor effect on subsonic ejector	-	Test Station	Primary flow, primary and secondary pressure	Current density, primary flow, power, entrainment and recirculated ratio	The comparison between the entrainment ratio and the mole recirculation ratio could express the effect of the water vapor on the actual quantity of recirculated hydrogen.	[16]
2017	Discrete ejector	-	Test Station	Current and power, secondary flow mole fraction	Stack and system efficiency, secondary pressure and temperature, entrainment ratio, voltage	The recirculation rate ranged from 2.6 to 1.6 at 25A and 160 A, respectively.	[15]

Chapter 2

Experiment

2.1 Setup

The experimental set-up consists of a test station designated by KTS, depicted in Figure 2.1. It encompasses all the equipment used to measure and control temperature, pressure, flow and relative humidity of hydrogen, H_2, and air. The temperature and flow of cooling water is also measured and controlled. KTS is used for performance measurement of stacks from 3 to 44 cells under different operating conditions. In order to conduct this work it was necessary to perform changes to the configuration of the test station. Two hydrogen recirculation loops were assembled as depicted in Figure 2.2. The inlet and outlet of the recirculation loop connect to the anode outlet and inlet of the PEMFC, respectively. The first loop, Figure 2.2 (a), consists on the active recirculation system and is composed by a drain vessel and a diaphragm hydrogen pump. A pressure regulator, a ball valve and a relief valve characterized in Section 2.1.2 were also installed. The relief valve protects the system from over-pressures and the pressure regulator on the active recirculation system allows setting the pressure to the working pressure of the PEMFC. The second loop, Figure 2.2 (b), consists on the passive recirculation system and is composed by a drain vessel and the venturi ejector. The ball valve present in both loops acts as a bleed

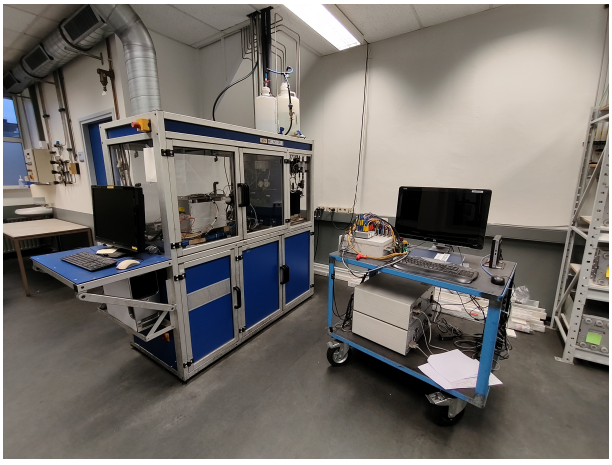

Figure 2.1: Test station: KTS.

valve allowing to purge nitrogen, N_2, and other undesirable gases that accumulate in the stack during operation as well as hydrogen after the experiment is conducted. The drain vessel used in both system retains major water droplets exiting the anode side of the fuel cell preventing, this way, anode flooding and the malfunctioning of both the diaphragm hydrogen pump and the venturi ejector. The latter are characterize in detail in Section 2.1.2.

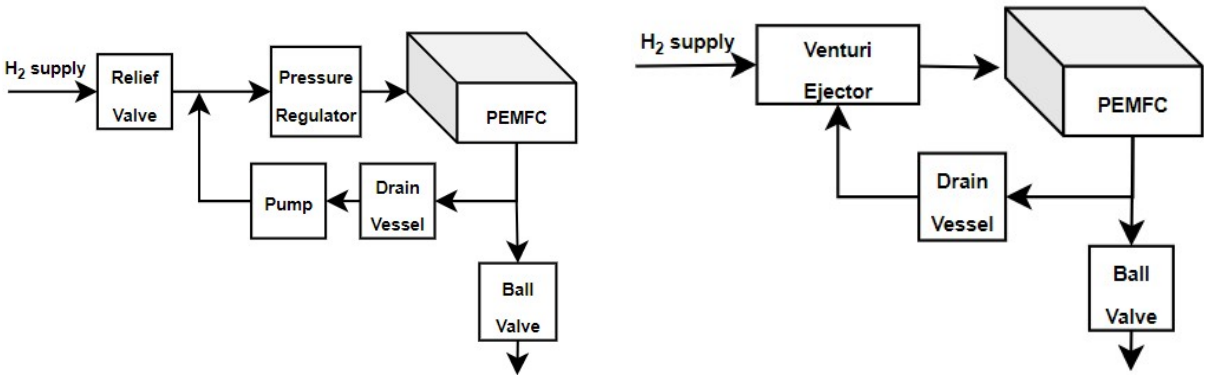

(a) Active recirculation (b) Passive recirculation

Figure 2.2: Active recirculation set-up scheme (a) and passive recirculation set-up scheme (b).

2.1.1 Nedstack®'s 5.5 kW PEMFC

The PEMFC allocated to this experiment consists of a Gen 2.51 with serial number S2397. It is composed by 44 cells with an active area of 200 cm^2 and a maximum power output of approximately 5.5 kW. At maximum power the PEMFC will consume 88 Nl/min of hydrogen, H_2, and 335 Nl/min of air. The optimal working temperature is 65℃. The I-V curve and the flow profiles of hydrogen, H_2, air and of the humidified hydrogen recirculated as a function of the current can be found in Chapter 3. This PEMFC was built for research purposes only. A simple specifications description of this PEMFC can be found in Figure 2.3. A commercial version that is closely comparable to this one is a FCS 5-HP which produces 5kW and a detailed specifications description can be found in Appendix A.

Specifications	
Model	Gen 2.51
Max.Power	5.5 kW @230V
Max.H2 flow	88 Nl/min
Max.Air flow	335 Nl/min
Active Area	200 cm^2 per cell
Cell count	44
Working Temp.	65℃
Weight	30 kg

Figure 2.3: Nedstack®'s 5.5 kW PEMFC specifications.

2.1.2 Recirculation System

The differentiator factor of this work relies on the implementation of two hydrogen recirculation systems, active and passive, in the test station, KTS, which allow to gather additional relevant data towards understanding the exact characteristics of the entrainment gas in both set-ups. Before this work, in order to humidify the dry hydrogen, it was flown through a bubbler. This increases the relative humidity, RH%, of the dry hydrogen, H_2, to the optimal level of 40% at stack temperature, 65℃. After flowing through the stack's anode, humidified hydrogen is released via proper channels to the atmosphere. Applying a recirculation loop in the anode makes this induced humidification redundant. As such, this component was suppressed from the system. Instead, the dry hydrogen, H_2, from the main supply and humidified hydrogen exiting the anode side of the PEMFC mix either in the t-joint after the diaphragm hydrogen pump or in the venturi ejector achieving this way a final mixture of hydrogen with an expected proper relative humidity, RH%, for optimal stack operation. Upstream these components, a drain vessel prevents water droplets from circulating in the loop and causing anode flooding and local hydrogen starvation.

Diaphragm hydrogen pump

Current operating systems use claw pumps to maintain a constant flow of hydrogen recirculating. For the 5.5 kW PEMFC in use, a 24 V KNF diaphragm pump with the part number N838KNDC fills the requirement of constantly flowing humidified hydrogen. It's product data sheet can be found in Appendix B. This value is obtained from the stack manual [42] as the set-point for the optimal operating conditions. In fact this pump recirculates, according to the specifications, 32 Nl/min which slightly increases the stoichiometry. As explained further ahead in Chapter 4 this does not originate a problem. Moreover, in the same chapter it is explained that the set-point of 25 Nl/min is in itself over-dimensioned for low currents. This fact means that a higher stoichiometry then needed is obtained in this range of operation. Nevertheless, it creates an opportunity to further increase the systems total efficiency if a better management of the energy used to power the pump can be done. In the case of this study, substituting an energy demanding device like a pump by a passive component like a venturi ejector completely eliminates the parcel of the system's efficiency decrease due to the use of a pump.

HyLoop®

After an extensive procurement process, HyLoop® was selected for a first approach to passive hydrogen recirculation within Nedstack. HyLoop® is a product of Ad-Venta INNOVATIVE. It has been successfully applied in a extensive range of PEMFC vehicles, from bicycles to drones. HyLoop® is a plug and play solution that integrates a control system that ensures the correct functioning of the venturi ejector. It's product data sheet can be found in Appendix C. It is composed by a proportional solenoid valve, a pressure relief valve, two pressure and one temperature sensors as well as a control unit. As depicted in Figure 2.4, the HyLoop® input (to the left) is connected to the main supply of dry hydrogen, H_2, the second inlet (to the bottom right) is connected to the anode exit, downstream the drain vessel. The outlet

is connected to the anode inlet. HyLoop® guarantees a minimum recirculation percentage of 50% and a maximum of 225% which means that at least half and a maximum of twice the input flow is recirculated. Since a stoichiometry of 1.25 is recommended for the anode side when in open-anode, 0.25 or 25% of the inlet flow will be recirculated when in a closed loop. In fact, as mentioned above, this value will be even higher in the case of the pump as well as in the case of HyLoop®.

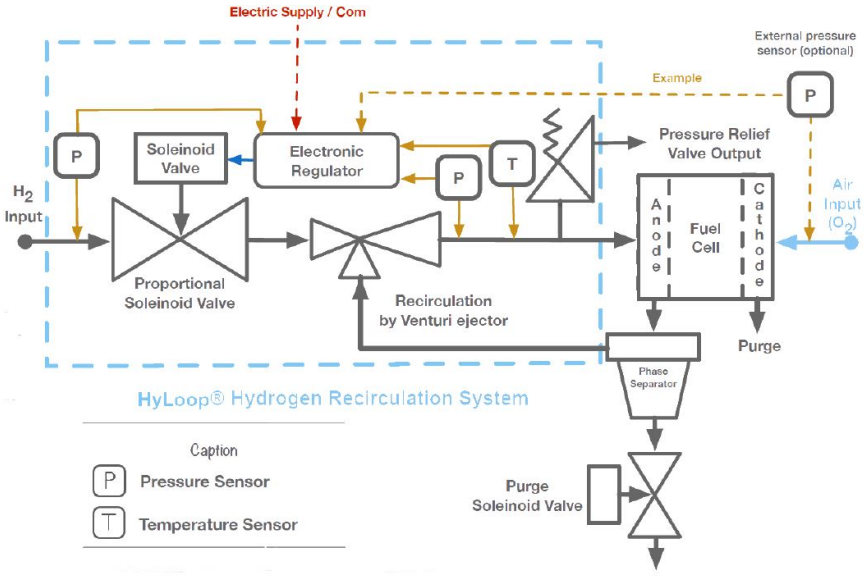

Figure 2.4: HyLoop®'s P&ID.

Pressure regulator

The pressure regulator with part number KPR 1DRB412E200H0 is manufactured by Swagelock®. It is manually set to the operating pressure of the PEMFC, 300 mbar.

Relief valve

The relief valve with part number SS-RL4S8 is manufactured by Swagelock®. It is set to open at a pressure of 700 mbar.

Ball valve

The ball valve with part number SS-12P6T-MM is manufactured by Swagelock®. It as the main function of allowing the flushing of the system.

Drain vessel

In order to remove water droplets formed on the cathode side of the PEMFC a DG111-223 drain vessel from Classic Filters is used. It has a capacity of 35 cc.

Gases

A network of compressed air at 8 bar is available in the building from which air flows into the PEMFC after passing a filter that removes most particles and having the pressure reduced to 450 mbar. Hydrogen with a purity of 99.999% supplied by HyGear® is stored in a Airliquide tank at 300 bar.

2.1.3 Acquisition System

The acquisition system is composed by pressure, temperature and humidity sensors on the anode inlet and outlet of the PEMFC in order to measure the differential between both terminals. Mass flow meters/controllers are placed upstream the entire system to measure the exact quantity of hydrogen, H_2, and air being consumed.

Mass Flow Meters

The flow of hydrogen, H_2, and air, is measured by EL-FLOW® flow meters from BRONKHORST. Hydrogen is supplied by a F-113AC-RAA-44-V model with a maximum flow of 500 Nl/min and handles a maximum pressure of 20 bar (g). Air is supplied by a F-202AC-RAB-55-V model with a maximum flow of 250 Nl/min and handles a maximum pressure of 6 bar (g). A LabView program in the computer of the KTS acts as the control unit for both equipment. Table 2.1 displays a summary of the specifications of the flow meters.

Table 2.1: Mass Flow Controllers specifications summary.

Specification	Hydrogen FM	Air FM
Manufacturer	BRONKHORST®	BRONKHORST®
Model	F-113AC-RAA-44-V	F-202AC-RAB-55-V
Max.Flow	500 Nl/min	250 Nl/min
Max.Pressure	20 bar (g)	6 bar (g)
Accuracy	±0,5% RD	±0,5% RD
Leakage	$<$2 x 10 e$^{-9} mbarl/sHe$	$<$2 x 10 e$^{-9} mbarl/sHe$

Temperature and Relative Humidity sensors

The integrated temperature and relative humidity sensors are based on CMOSens® technology. The signal from the sensor is sent to and from the comsensor to the computer where Sensirion software displays the values read. The sensor was previously incorporated in a 5 mm thread couple and a hole with the same dimensions had been made on the PEMFC connectors in order to screw it. Table 2.2 displays a summary of the specifications and Figure 2.5 depicts the assembly of the sensors.

Pressure Sensors

Pressure sensors are already incorporated in the KTS. These are testo ® 6349 pneumatic electrical transmitters that measure positive, negative and differential pressure. A pressure cell in the sensor

Table 2.2: Temperature and RH% sensors specifications summary.

Specification	RH% Sensor	Temperature sensor
Manufacturer	Sensirion	Sensirion
Model	SHT75	SHT75
Range	0-100%	-40℃-123.8℃
Accuracy	±2% (10%-90% RH%)	±0.5℃ (5℃-40℃) ±0.9℃ (-15℃-60℃)
Response time	3 s	5 s - 30 s
Resolution	0.03% RH%	0.01℃

(a) Assembly overview (b) Detailed assembly view

Figure 2.5: Temperature and RH% sensors assembly.

encompasses a membrane spring that moves between two chambers of the pressure cell. Table 2.3 displays a summary of the specifications and Figure 2.6 depicts the assembly of the sensors.

Table 2.3: Pressure sensor specifications summary.

Specification	Pressure Sensor
Manufacturer	testo
Model	6349
Range	0 - 0.5 bar
Accuracy	±3.0 × $10^{-6} bar$
Medium	Air, all non-corrosive

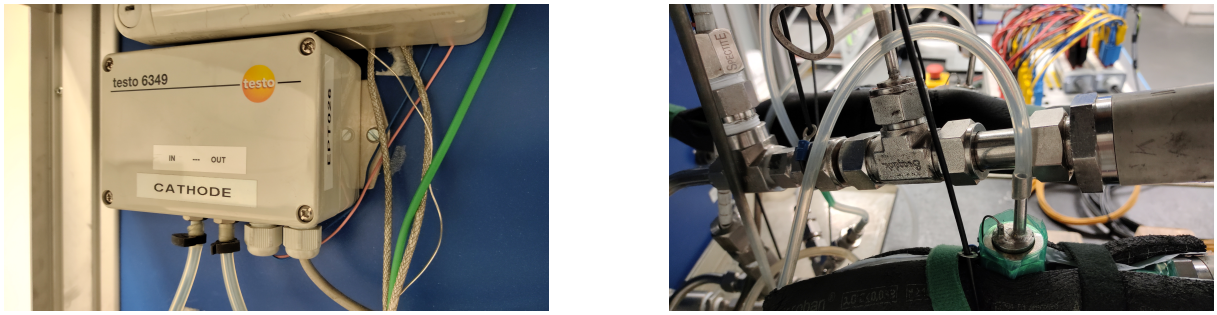

(a) Pressure transmitter (b) Sample point

Figure 2.6: Pressure sensors assembly.

2.2 Instruments calibration and regulation

Relief valve regulation

Although the maximum recommended pressure in the anode is 450 mbar,[42], the pressure was instead set to 700 mbar which corresponds to the minimum pressure set-point allowed by the valve used. This as to do with the fact that this was a valve available in the laboratory making it unnecessary to order a new one. In order to set the Swagelock®'s relief valve pressure, the nut on top of the valve is tightened or loosen, respectively increasing or decreasing the pressure set point at which the fluid can escape. To start the procedure, the relief valve is tightened as much as possible making the pressure at which the gas escapes too high when compared with the working pressure of the system, 300 mbar. A manometer present in the pressure regulator downstream the pressure relief valve is set to 700 mbar helping measuring and setting the pressure desired on the relief valve. Once the pressure is set in the pressure regulator to 700 mbar, the nut from the relief valve is continuously loosen until a drop in pressure is observed on the manometer. This pressure drop indicates that gas is escaping at some point upstream the system, in this case, escaping trough the relief valve. A second relief valve is used in this work, it belongs in the passive recirculation loop and is already incorporated in the HyLoop®. It was factory-set to 450 mbar.

Venturi ejector regulation

HyLoop® encompasses a control unit that allows the user to set the desired outlet pressure of hydrogen. The pressure setting is done recurring to a PEAK connection. Using the software provided by the manufacturer, HyLoop2020CanMonitoring® and introducing the desired outlet pressure of 300 mbar, the feed-back loop between the pressure sensor downstream, the control unit and the proportional valve upstream guarantees the constant output pressure. A 120 Ω resistance was used between the PEAK and HyLoop® in order to make the connection between both components stable. This is a common practice when dealing with CAN-BUS communication. CAN High (red wire) was connected to port 7 and CAN Low (black wire) was connected to port 2 of a DB-9 connector. Figure 2.7 depicts the assembly.

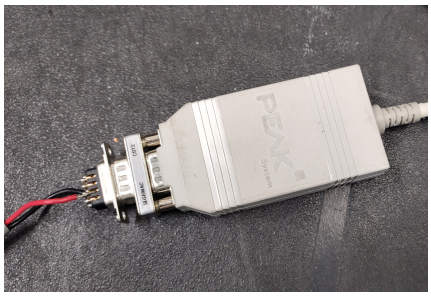

Figure 2.7: CAN-BUS interface: PEAK with 120 Ω DB9 connector.

Mass Flow meter

In order to verify the correct functioning of the 500 Nl/min mass flow meter, a comparative approach was undertaken, Figure 2.8. To accomplish this, the flow-meter was mounted in series with the KTS's embedded flow-meters and the readings were compared. Both values read were the same for a sample of three points, 15 Nl/min, corresponding to the minimum anode flow in the fuel cell, 38 Nl/min and 61 Nl/min, the latter corresponding to the maximum operating point studied. This allows to conclude with an acceptable degree of confidence that the readings from the 500 Nl/min flow-meter are reliable.

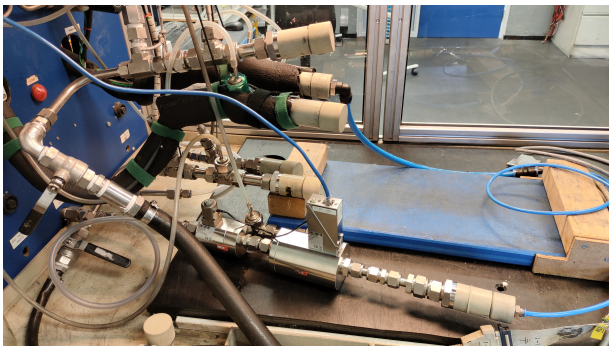

Figure 2.8: Flow meter readings validation assembly.

Pressure Sensors

In order to verify the correct functioning of the pressure sensors mounted in the KTS, a comparative approach was undertaken. The reading given by the testo ® 6349 was compared to the reading of the pressure regulator in the pump set-up and to the reading of a second pressure sensor that was mounted in the circuit for this purpose, Figure 2.9. All three values read were the same, meaning 300 mbar. This allows to conclude with an acceptable degree of confidence that the readings from the testo ® sensors are reliable.

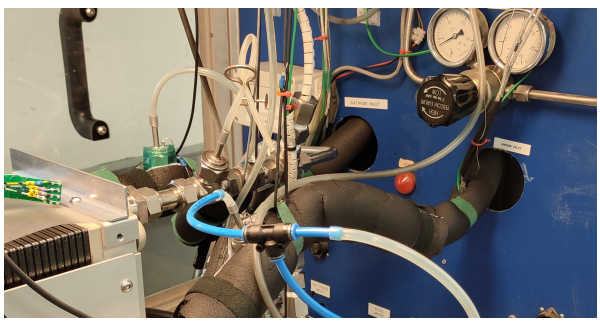

(a) Sample point

(b) Auxiliary pressure sensor

Figure 2.9: Pressure sensors readings validation assembly.

Temperature and RH% sensors

The temperature and relative humidity sensors readings were verified via comparative approach. The sensors were placed inside temperature and relative humidity controlled rooms within Nedstack®'s building. The rooms are used to keep MEAs conditioned at constant atmospheric conditions. The set-points measured are present in Table 2.4.

Table 2.4: Temperature and RH% sensors readings validation.

	Temperature1 (ºC)	Humidity1 (%)	Temperature2 (ºC)	Humidity2 (%)	Temperature (ºC)3	Humidity3 (%)
Reference Sensor	20.52	37.20	22.72	35.33	24.48	33.72
Sensor 1	21.55	34.31	22.57	35.09	23.86	33.64
Sensor 2	21.27	34.99	22.43	35.02	23.69	34.20

Analysing the results it's verified that there is a small variance between the Reference Sensor and Sensors 1 and 2 as well as there is a small variance between Sensor 1 and 2 themselves in sample point 3. These variances could have been caused by local differentiated characteristics of the air to which the sensors respond due to their high resolution. Nevertheless, since the stack accepts a wide operating range of hydrogen inlet humidity and temperature, between 40-100% humidity at stack temperature and 60-70ºC, the use of these sensors was still considered acceptable.

2.3 Procedure

A test plan for the experiments carried out was designed and can be seen in detail in Appendix D. Two groups of experiments were performed, ahead designated by G1 and G2, respectively. G1 corresponds to 3 sets of I-V curves (basic performance) for the three system set-ups and G2 to three start-up/shut-down sequences for all set-ups and three ramp-up/ramp-down sequences also for the three set-ups. Table 2.5 summarizes the tests performed.

Table 2.5: Groups of tests performed.

G1 - I-V Curve (basic performance) tests	G2 - Stress tests
3 x Open Anode (no recirculation)	3 x Open Anode, Active and Passive start-up/shut-down
3 x Active recirculation	3 x Open Anode, Active and Passive ramp-up/ramp-down
3 x Passive recirculation	

2.3.1 G1 - I-V Curve tests

Open Anode (no-recirculation)

After installing the PEMFC in the KTS and connecting all the piping and electrical cables, the test battery B1 is ready to start. The temperature of the PEMFC is increased to the operation set-point of 65℃ by passing hot water from an external source trough the cooling conducts of the PEMFC. Once it reaches the required temperature both the anode and cathode are flushed with nitrogen, N_2, in order to clear the

channels of any other gases and water droplets. Afterwards, hydrogen floods the anode side and air the cathode side bringing the stack to OCV. At this point a load controlled by LabView is used to draw a user defined current from the PEMFC. The current is firstly increased to 40 A and afterwards from 40 A to 160 A in steps of 20 A filling the template table in Appendix D. At this point the heat source heating the cooling water as already been turned off and the flow adjusts automatically to keep a constant inlet temperature of 65 ℃.

Active recirculation

For active recirculation, the subsystem presented in Figure 2.10 is mounted according to the scheme in Section 2.1, Figure 2.2 - (a). Using a closed anode obliges to perform a few changes to the KTS namely the installation of a low pressure regulator that regulates the anode inlet pressure to 300 mbar (the working pressure of the PEMFC). A relief valve regulated to 700 mbar is also included to prevent over pressures upstream the system. Adding to this, a needle valve is also mounted downstream the anode in order to allow flushing of hydrogen and nitrogen. The process of heating up the PEMFC to 65 ℃ is then repeated. In this case, the 500 Nl/min flow-meter from BRONKHORST is mounted in the KTS due to the reasons explained in Section 2.1.3. Nitrogen flush is not performed since it was not possible to connect the added 500 Nl/min flow-meter to the nitrogen supply. Instead, a hydrogen flush is performed. At this point, the needle valve is closed to increase pressure of the anode from 42 mbar (open anode pressure) to 300 mbar. The hydrogen recirculation pump is then turned on initiating the gas recirculation. The current is again increased from 40 A to 120 A in steps of 20 A and the template table in Appendix D is filled.

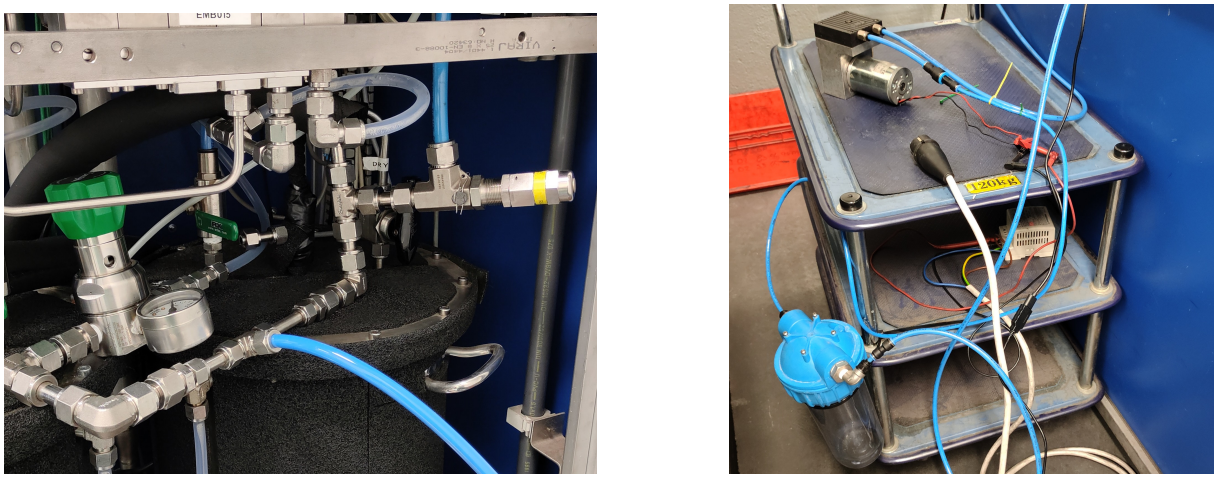

(a) Low pressure regulator and pressure relief valve

(b) Drain vessel and hydrogen recirculation pump

Figure 2.10: Active recirculation system assembly.

Passive recirculation

For passive recirculation, the subsystem presented in Figure 2.11 is mounted according to the scheme in Section 2.1, Figure 2.2 - (b). In this case, the 500 Nl/min flow-meter is again used. HyLoop®, en-

compasses a proportional solenoid valve upstream the ejector and regulates the pressure downstream the ejector opening and closing this valve. A pressure sensor downstream the ejector completes the feedback loop. This means that the low pressure regulator is dispensable in this case. Since a pressure relief valve is also encompassed in the HyLoop®the relief valve from the previous test is also dispensable. The needle valve is maintained in the system. The process of heating up the PEMFC to 65℃ is then repeated. After reaching the required temperature, hydrogen floods the anode and air the cathode. Anode flush is performed with hydrogen to clear any water droplets and undesired gases and the needle valve is closed to increase pressure of the anode from 42 mbar (open anode pressure) to 300 mbar. Given the fact that the HyLoop®is a mechanical device, gas recirculation is initiated as soon as current is drawn from the stack. The current is again increased from 40 A to 120 A in steps of 20 A and the template table in Appendix D is filled.

(a) 500Nl/min flow meter

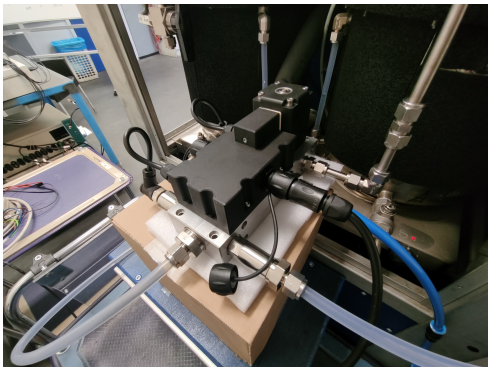

(b) HyLoop®

Figure 2.11: Passive recirculation system assembly.

2.3.2 G2 - Stress tests

Open Anode, Active and Passive start-up/shutdown

After installing the PEMFC in the KTS and connecting all the piping and electrical cables, the test sequence B2 is ready to start. The temperature of the PEMFC is again increased to the operation set-point of 65℃ by passing hot water trough the cooling conducts of the PEMFC. Nitrogen is used to flush the anode in the Open Anode set-up and hydrogen is used in both the other cases. Hydrogen floods the anode side and air the cathode side generating an open circuit voltage on the stack terminals. At this point, the start-up procedure is initiated. Data after stabilization is extracted at 0 A and afterwards at 40 A. The reserve operation is conducted to analyse the shut-down procedure.

Open Anode, Active and Passive ramp-up/ramp-down

After installing the PEMFC in the KTS and connecting all the piping and electrical cables, the test sequence B2 is ready to start. The temperature of the PEMFC is again increased to the operation set-point of 65℃ by passing hot water trough the cooling conducts of the PEMFC. Nitrogen is used to flush the

anode in the Open Anode set-up and hydrogen is used in both the other cases. Hydrogen floods the anode side and air the cathode side generating an open circuit voltage on the stack terminals. At this point, the ramp-up, rump-down procedure is initiated. Data after stabilization is extracted at 40 A and afterwards at 120 A. The reserve operation is conducted to analyse the rump-down procedure.

Chapter 3

Models

3.1 Fuel cell dynamics

In the case of the PEMFCs produced by Nedstack®, models were extracted and normalized from experimental measurements. Details of the most important numerical simulations performed in this work are described hereafter in Section 3.2. These simulations describe the most important factors to be controlled by the end user in order to achieve the correct functioning of the PEMFC. Moreover, these factors are all described as a function of the current. Additional factors, described in [42], can be simulated and studied in order to better understand the specific behaviour of a given Nedstack® PEMFC.

3.2 Influenced factors vs. current

3.2.1 Anode

Hydrogen Inlet Flow, $\dot{V}_{H_2inlet}$

The inlet flow of a stack accounts for the amount of hydrogen needed for the correct operation of a stack at a given current. Equation 3.1 describes the behaviour of hydrogen inlet flow as the current produced by the stack increases. Equation 3.2 accounts for the minimum amount of hydrogen that should be supplied to the stack at any point of operation. It depends only on the number of cells of the stack, n, which in this case equals 44.In Equation 3.1, the factor 1.25 accounts for the minimum stoichiometry at which hydrogen should be supplied to the stack. It is greater than one due to the reasons presented in Section 1.3. The influence factor, n, represents the number of cells that constitute the stack and I stands for the current produced by the stack.

$$\dot{V}_{H_2inlet} = 1.25 \times 10^{-3} \times n \times I \ \ (Nl/min) \qquad I > 40A. \tag{3.1}$$

$$\dot{V}_{H_2mininlet} \geq 0.6 \times n \ \ (Nl/min) \qquad I \leq 40A. \tag{3.2}$$

Hydrogen Recirculation

Present PEMFC systems use an active hydrogen recirculation. The hydrogen recirculation pump operates in steady state for the entire range of operation of the PEMFC. This means that recirculation of hydrogen is performed in excess in the entire span of operation. Equation 3.3 describes its behaviour. The factor 2.5 accounts for the stoichiometry of recirculated hydrogen, n, represents the amount of cells in the stack and I_{max} stands for the maximum recommended current produced by stack, 230 A.

$$\dot{V}_{H_2recycled} = 2.5 \times 10^{-3} \times n \times I_{max} \ \ (Nl/min). \tag{3.3}$$

Hydrogen Consumption

The amount of hydrogen consumed in the stack is given by Faraday's law which can be translated for this stack in Equation 3.4.

$$\dot{V}_{H_2consumed} = 6.965 \times 10^{-3} \times n \times I \ \ (Nl/min). \tag{3.4}$$

Hydrogen Respiration

Hydrogen respiration accounts for the amount of hydrogen that escapes the stack by infiltration. This quantification depends only on the number of cells, n, and is given by Equation 3.5.

$$\dot{V}_{H_2respiration} = 0.593 \times 10^{-3} \times n \ \ (Nl/min). \tag{3.5}$$

Anode Pressure Drop

The stack pressure drop increases linearly with the inlet gas flow. Equation 3.6 gives the typical anode pressure drop for the stack under normal operating conditions. Equation 3.7 gives the minimum pressure drop in the anode.

$$\Delta P_{H_2} = 0.2 \times I + 1.4 \ \ (mbar) \qquad I > 40A. \tag{3.6}$$

$$\Delta P_{H_2} = 15 \ \ (mbar) \qquad I \leq 40A. \tag{3.7}$$

3.2.2 Cathode

Air Inlet Flow

The inlet flow of air in a stack accounts for the amount of air needed for the correct operation of a stack at a given current. Equation 3.8 describes the behaviour of the air inlet flow as the current produced by the stack increases. Equation 3.9 accounts for the minimum amount of air that should be supplied to the stack at any point of operation. It depends only on the number of cells of the stack, n, which in this case equals 44.

$$\dot{V}_{airinlet} = 1.25 \times 10^{-3} \times n \times I \ \ (Nl/min) \qquad I > 40A. \tag{3.8}$$

$$\dot{V}_{airmininlet} \geq 1 \times n \ \ (Nl/min) \qquad I \leq 40A. \tag{3.9}$$

Oxygen Consumption

The amount of oxygen consumed in the stack is given by Faraday's law which can be translated for this stack in Equation 3.10, where, n, represents the number of cells of the stack and I stands for the current produced by the stack.

$$\dot{V}_{O_2consumption} = 3.483 \times 10^{-3} \times n \times I \ \ (Nl/min). \tag{3.10}$$

Air Pressure Drop

The stack pressure drop in the cathode increases linearly with the inlet flow. Equation 3.11 gives the typical cathode pressure drop for the stack under normal operating conditions. Equation 3.12 gives the minimum pressure drop in the cathode.

$$\Delta P_{Air} = 0.2 \times I + 1.4 \ \ (mbar) \qquad I > 40A. \tag{3.11}$$

$$\Delta P_{Air} = 15 \ \ (mbar) \qquad I \leq 40A. \tag{3.12}$$

3.2.3 Venturi Ejector

The equations that rule the behaviour of hydrogen in the ejector present in the HyLoop® are not known due to the fact that these are proprietary technology of Ad-venta®. Nevertheless, a relation between the recirculation ratio and the injected flow was provided together with the product's datasheet and is shown in Figure 3.1. According to the manufacturer, the minimum recirculation ratio of the ejector corresponds to 50% of the injected flow, represented by the black dotted straight line. However, the recirculation ratio of the ejector is expected to be much higher as shown by the orange curve originating a stoichiometry of about 3.25 in the operational region of interest, 40-160 A, that corresponds an ejected flow between 10-60 Nl/min. This graphic was experimentally obtained for 100% dry hydrogen, H_2, and for 100 mbar pressure drop at Ad-Venta's test bench. Equation 3.13 represents an extrapolated equation obtained from this graph where phi, Φ, is the recirculation ratio and $\dot{V}$ represents the ejector's inlet flow.

$$\Phi = -0.012\dot{V}_{H_2inlet} + \dot{V}_{H_2inlet} + 207 \ \ (\%). \tag{3.13}$$

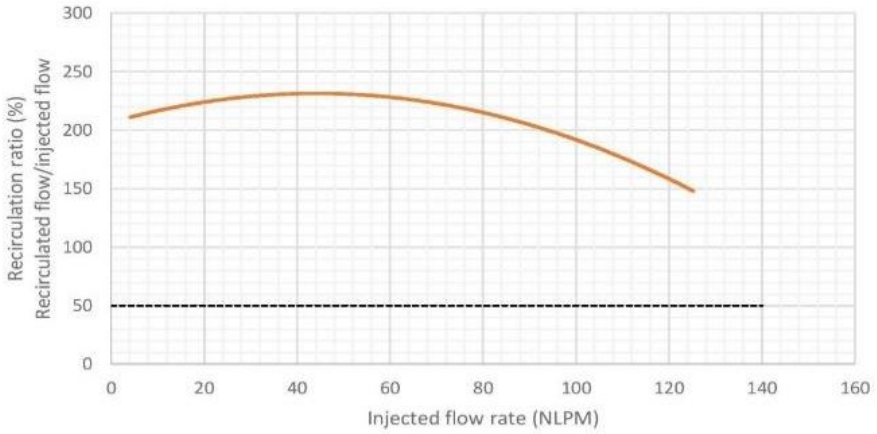

Figure 3.1: HyLoop®'s performance curves. As in Appendix C.

3.3 PEMFC I-V Curve

The I-V curve, or polarization curve, is the most common method of characterizing a fuel cell. A reliable curve requires stable operating conditions. These depend among other factors, on the reliability of the components that constitute the BOP. It implies that a change in the operating conditions, meaning, a change of components in the BOP will have an impact in the I-V curve, specially on its stability over time. Thus, a way of validating the use of BOP components is to verify the stability of the I-V curves that different BOP set-ups generate. For this study the different sample points described in Section 2.3 were taken every 2 minutes. The proximity of the curves should provide a good indication towards validating a new set-up. The I-V curve taken as reference is the one obtained from a DQC (Detailed Quality Control) test of the stack, Figure 3.2. DQC is the standard test used for product approval. It is performed with open anode and consists of drawing a fixed current from the fuel cell and measuring the output voltage. In this case the current is varied from 0A to 298A. For this stack, in normal operation, the current drawn should stay within 40A to 230A, in order to extend its lifetime.

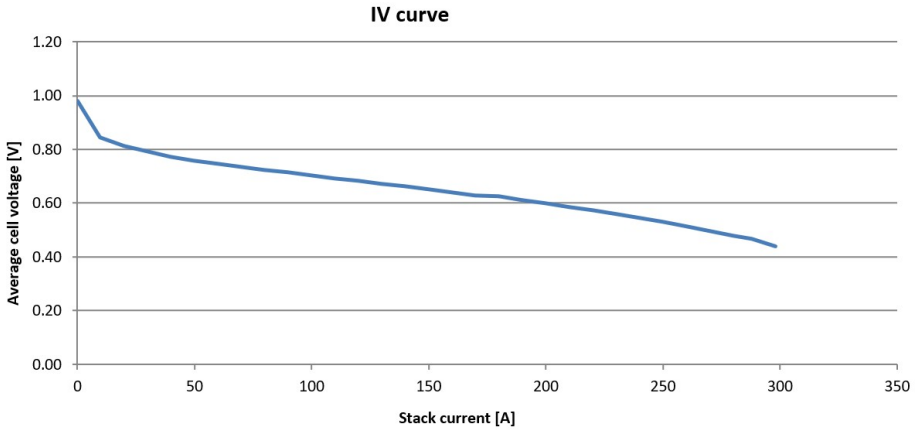

Figure 3.2: Stack's I-V curve obtained from the DQC test @1.25 stoichiometry in the anode and @2.0 stoichiometry in the cathode. PEMFC @65℃.

Chapter 4

Results and Discussion

An analysis of the results from the conducted experimental tests is performed. First, an analysis of the influence of the three set-ups: open-anode, pump-driven and ejector-driven recirculation on the inlet relative humidity , $HR\%_{H_2inlet}$, on inlet gas temperature, T_{H_2inlet}, on the pressure difference, ΔP_{Anode}, of the anode, and on the dry hydrogen inlet flow, $\dot{V}_{H_2inlet}$, is performed. Then, the impact of ejector-driven recirculation on the start-up/shut-down procedure is analysed and afterwards, the ejector response time on ramping up and ramping down. Finally, a brief comparison between the efficiencies of pump-driven and ejector-driven recirculation is performed.

4.1 Influenced factors characterization for all set-ups

The efficiency of a PEM fuel cell depends on an extensive list of factors. This study focused on the inlet gas mix relative humidity and temperature, anode and cathode pressure drops and consumed and recirculated hydrogen flow rate. These factors were measured when operating the KTS with a hydrogen recirculation pump, an ejector and an open anode set-up.

4.1.1 I-V Curve

The stack used for this project was built for research purposes only, therefore, no theoretical/extrapolated I-V curve can be attributed. To solve this problem, the BoL I-V curve was used. This I-V curve is obtained through a procedure called DQC. It consists of characterizing a new stack with different parameters including an I-V curve.

Therefore, the open anode, pump and ejector's I-V curves obtained with the KTS were compared to the BOL I-V curve and to a 5-HP kWe and 7-XXL kWe stack I-V curves, both commercial stacks. Figure 4.1 presents the I-V curves obtained for all tests conducted. A first qualitative analysis shows that the I-V curves from all set-ups fall in the expected area of performance, meaning between the 5-HP kWe and 7-XXL kWe stack I-V curves.

Furthermore, it is visible that the open anode, pump and ejector I-V curves fall very close together and close to the BOL I-V curve. In fact, the stack looks to be in a good condition given that the open anode

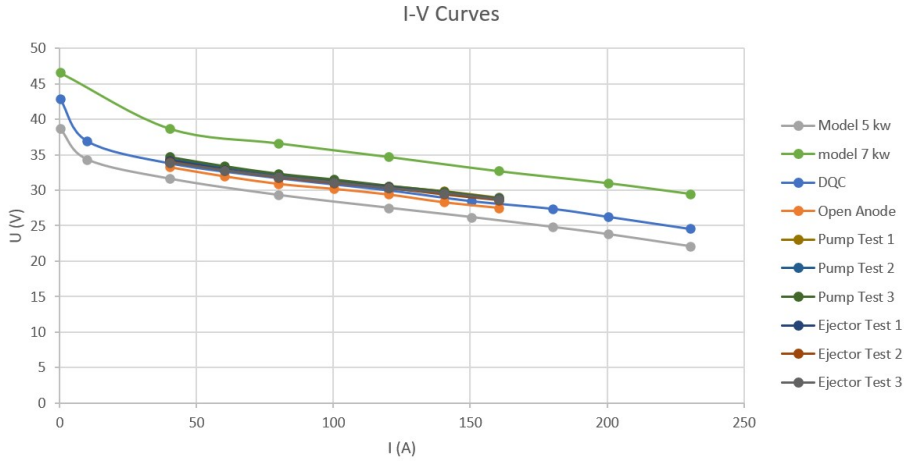

Figure 4.1: Experimental I-V curves collected for all three set-ups: OA @1.25 stoichiometry, Ejector and Pump @1.0 stoichiometry compared to 5kW and 7kW model I-V curves. PEMFC @65℃.

I-V curve seems to match almost perfectly the BOL I-V curve. A more thorough analysis of the results shows an average difference between voltage values of the two I-V curves of 2%. This value brings more relevance to the results further obtained given the fact that these won't be significantly affected by decaying effects on the stack. Figure 4.2 depicts an average of the I-V curves of the pump and the ejector compared to the 5-HP kWe and 7-XXL kWe stack I-V curves. A brief analysis of the curves seems to indicate a satisfactory operation of the stack with both set-ups. The average relative errors between the pump and ejector average curves when compared to the DQC curve are 2.1% and 1.1%, respectively. The absolute average difference voltage between both set-ups is 0.3 V. These results are summarized in Table 4.1.

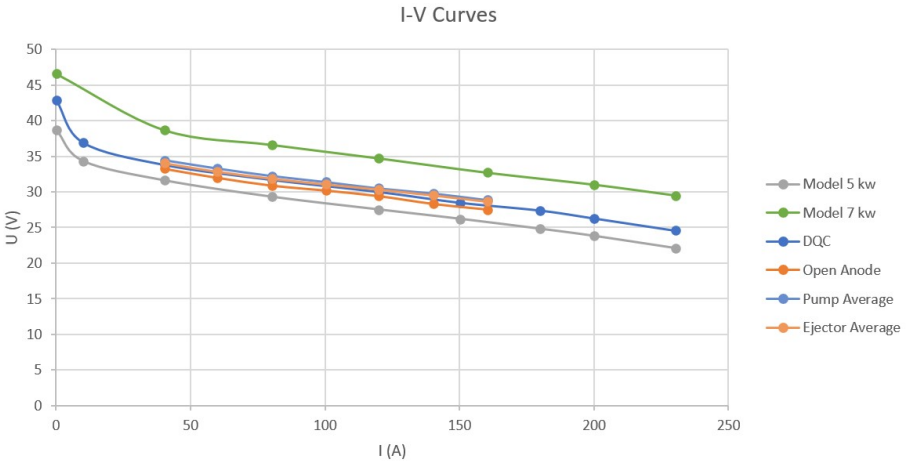

Figure 4.2: Experimental averaged I-V curves collected for all three set-ups: OA @1.25 stoichiometry, Ejector and Pump @1.0 stoichiometry compared to 5kW and 7kW model I-V curves. PEMFC @65℃.

4.1.2 Hydrogen Inlet, $\dot{V}_{H2inlet}$

The consumption of Hydrogen is expected to have significantly different values when recirculation is in place when compared to the model supplied in the stack manual [42] and described in Section 3.2. As

Table 4.1: Relative deviation of the average I-V curves collected for all three set-ups: OA, Ejector and Pump compared to the DQC curve. Maximum absolute deviation between the average I-V curves of the pump and the ejector.

$\delta_{(OA-DQC)}$	$\delta_{(Pump-DQC)}$	$\delta_{(Ejector-DQC)}$	$\Delta_{(Pump-Ejector)}$
2%	2.1%	1.1%	0.3 V

with the test station used, the stack manual considers the use of the fuel cell in open-anode, although it is not the case when a stack integrates a system. The stack manual considers a stoichiometry of 1.25 for the hydrogen supply. As explained in Chapter 3 this means that hydrogen is supplied in excess by 25%. The excess hydrogen prevents harmful occurrences such as hydrogen starvation in the cells, explained in Chapter 1. In open-anode operation this amount of hydrogen is not consumed and as such, it is released to the atmosphere.

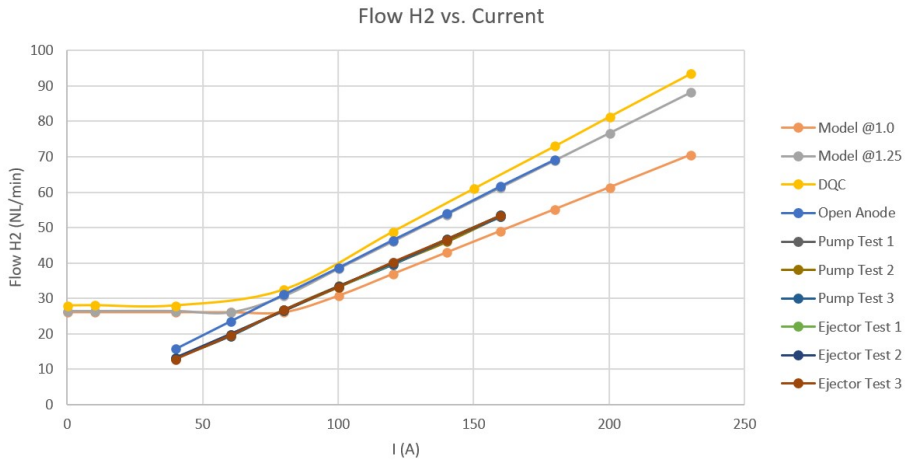

Figure 4.3: Experimental results for hydrogen flow consumption collected for all three set-ups: OA, Ejector and Pump compared to DQC and the extrapolated model as described in Section 3.2 at 1.0 and 1.25 stoichiometry. PEMFC @65℃.

Implementing a recirculation system means that only the flow of hydrogen being consumed is being supplied to the stack resulting in a stoichiometry of 1.0. Figure 4.3 precisely shows this effect in a first analysis. The hydrogen consumption curve for both set-ups, pump and ejector, lies in the region that was expected, meaning below the DQC and the open-anode curves. It is possible to see in the figure that the hydrogen flow rate curves from the six tests run fall closer to the I-V curve model at 1.0 stoichiometry than to the 1.25 stoichiometry. In fact, the average relative difference between the DQC hydrogen consumption and the pump and ejector set-up's hydrogen consumption is -20.2% and -19.9% respectively, meaning this percentage is being saved just by adding a recirculation system. It is also possible to observe that the flow rate profiles seem almost coincident indicating a good reproducible of the results with both set-ups. Furthermore, the fact that the profiles from both devices seem to overlap provides a positive indication towards the possibility of replacing the pump for the ejector.

Figure 4.4 depicts an average of the hydrogen consumption of the pump and the ejector. Considering the area of interest between 80 A and 160 A, the average relative difference between the Model @1.0 and the pump and ejector set-up is 2.4% and 2.8%, respectively. An interesting point worth noticing is

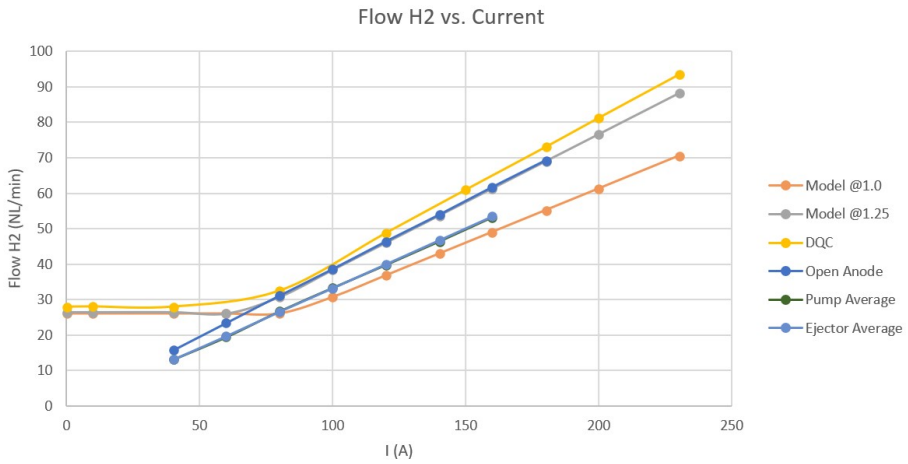

Figure 4.4: Experimental results for average hydrogen consumption collected for all three set-ups: OA, Ejector and Pump compared to DQC and the extrapolated model as described in Section 3.2 at 1.0 and 1.25 stoichiometry. PEMFC @65℃.

the fact that the relative difference between both set-ups and the 1.0 stoichiometry model is not 0%. There must be a reason for this result but only possible reasons could be identified. First, there could be a leakage at some point in the system although it was scanned with a hydrogen sensor multiple times and always indicated a very low and safe percentage of hydrogen concentration in the air, not sufficient to lead to this difference. The hydrogen consumption absolute average difference between the pump and ejector set-up is 0.26 Nl/min. This is a considerably low value and as such does not represent a relevant meaning. In fact it is 100x smaller than the flows being measured at low currents and 250x smaller than the flows at high currents. The meaningful results of this measurements are summarized in Table 4.2. Overall, these results show a positive tendency towards the possibility of replacing the pump for the ejector.

Table 4.2: Average relative errors of the hydrogen flow consumption collected for all three set-ups: OA, Ejector and Pump compared to the DQC curve and maximum absolute deviation between the average I-V curves of the pump and the ejector.

$\delta_{(OA-DQC)}$	$\delta_{(Pump-DQC)}$	$\delta_{(Ejector-DQC)}$	$\delta_{(Model@1.0-Pump)}$	$\delta_{(Model@1.0-Ejector)}$	$\Delta_{(Pump-Ejector)}$
-6.8%	-20.2%	-19.9%	2.4%	2.8%	0.26 Nl/min

4.1.3 Air Inlet, $\dot{V}_{Airinlet}$

Air circulation in the cathode is independent from having hydrogen recirculation in place or not. Therefore it is expected that the air flow in the cathode varies in the same manner for all three set-ups. Figure 4.5 depicts that. A brief visual analysis suggests an almost complete coincidence of data points. Worth noting the significant deviation in the $\dot{V}_{Airinlet}$ profile of Pump Test 2 at current, I, equal to 120 A. As described in Section 2.3, the air flow meter/controller is controlled manually. The user needs to order the device to increase the opening of the control valve which most likely was not done properly in this case leading to a shortage of air flow rate. Nevertheless, this misuse of the equipment does not affect

the performance of the stack for the flow rate of air is as in the case of hydrogen supplied in excess. The only consequence out of it is a decrease of stoichiometry in the cathode. The data extracted in this point shows a stoichiometry decrease from 2.03 at 100 A to 1.83 at 120 A.

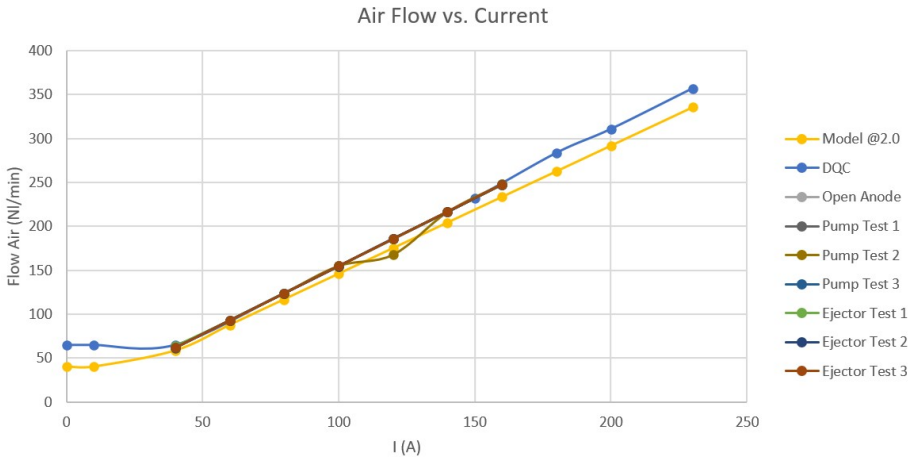

Figure 4.5: Experimental results for air consumption collected for all three set-ups: OA, Ejector and Pump compared to DQC and the extrapolated model as described in Section 3.2 at 2.0 stoichiometry. PEMFC @65℃.

In order to facilitate processing the data, an average of the $\dot{V}_{Airinlet}$ curves of the pump and the ejector was obtained and is depicted in Figure 4.6. As expected it shows an almost coincidence of points apart for the one at current, I, equal to 120 A, for the reasons explained above. A thorough analysis which results are presented in Table4.3 shows that the pump set-up presents a 0.6% and a 5.5% average deviation between the DQC and Model @2.0, respectively and the ejector set-up shows a 0.1% and 6% average deviation between the DQC and Model @2.0, respectively.

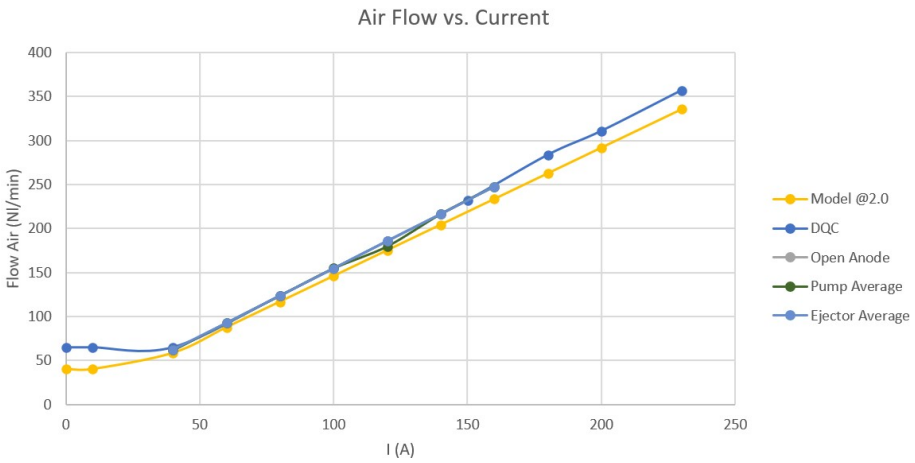

Figure 4.6: Experimental average results for air consumption collected for all three set-ups: OA, Ejector and Pump compared to DQC and the extrapolated model as described in Section 3.2 at 2.0 stoichiometry. PEMFC @65℃.

Table 4.3: Average relative deviations of the air flow consumption collected for all three set-ups: OA, Pump and Ejector compared to the DQC and the extrapolated model at 2.0.

$\delta_{(OA-DQC)}$	$\delta_{(Pump-DQC)}$	$\delta_{(Ejector-DQC)}$	$\delta_{(Pump-Model@2.0)}$	$\Delta_{(Ejector-Model@2.0)}$
0.7%	0.6%	0.1 %	5.5%	6%

4.1.4 Relative Humidity and Temperature

As discussed in Section 1.3, hydrogen recirculation plays a key role in humidifying the cells membrane. According to the stack manual [42], hydrogen inlet humidity should be kept at least at 40% at stack temperature, 65℃. Figure 4.7 and Figure 4.8 depict, respectively, the behaviour of the relative humidity and temperature of the inlet hydrogen entrainment as the current increases. Figure 4.7 shows immediately a difference between the behaviour of the RH% of the pump and ejector.

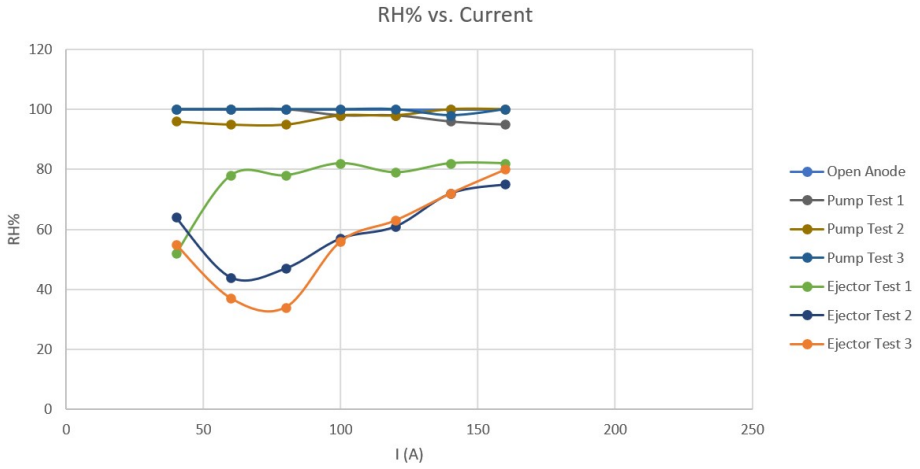

Figure 4.7: Experimental results for relative humidity collected for all three set-ups: OA @1.25 stoichiometry, Ejector and Pump @1.0 stoichiometry. PEMFC @65℃.

The pump originates a RH% similar to the open-anode and around 100%, according to the graph, whereas the RH% profile of the ejector tests is situated between 40-80%. Regarding Figure 4.8, it is possible to observe that the entrainment gas tends to an average temperature of 35℃ as the current, I, increases. Nevertheless, a detailed analysis of this data must be done. The fact that the results from these two set-ups are in the proximity of the upper limit of the measurement scale of sensors used requires considering that the RH% could actually be higher than 100%. In order to easily analyse these values, the average of the RH% and temperature curves of the two set-ups was considered and presented in Figure 4.9 and Figure 4.10.

Recurring to the figures it is clearly observed that the RH% of the open-anode and pump set-ups is in the upper limit of what the sensors can measure and that the profile of the RH% of the ejector set-up seems to increase as the current increases. Regarding Figure 4.10, it's possible to conclude that the temperature of the open-anode set-up is relatively stable and just below 55℃ and that the temperature profiles of both the pump and the ejector set-ups tend to 35℃ approximately. This means that exist

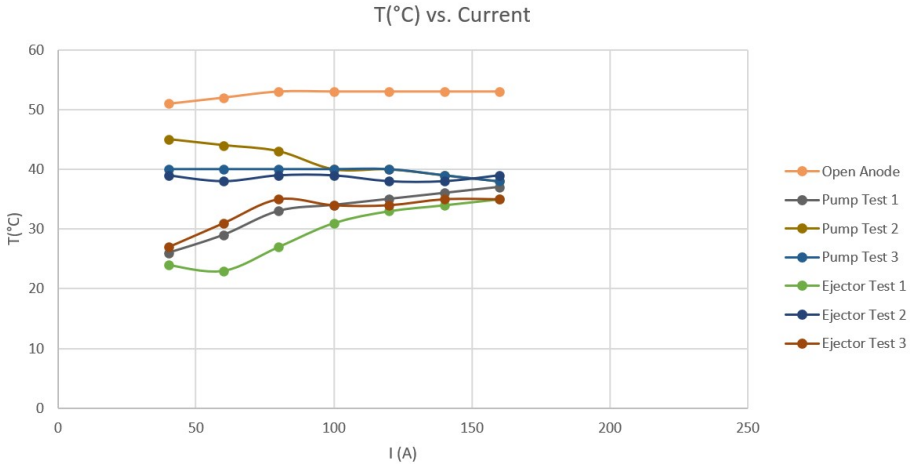

Figure 4.8: Experimental results for inlet temperature collected for all three set-ups: OA @1.25 stoichiometry, Ejector and Pump @1.0 stoichiometry. The value of temperature is itself an average of both sensors in series. PEMFC @65℃.

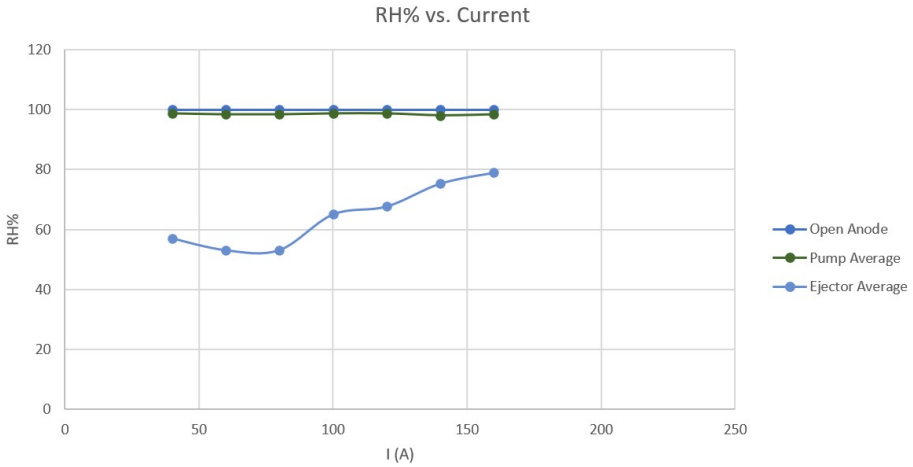

Figure 4.9: Experimental results for average relative humidity collected for all three set-ups: OA @1.25 stoichiometry, Ejector and Pump @1.0 stoichiometry. PEMFC @65℃.

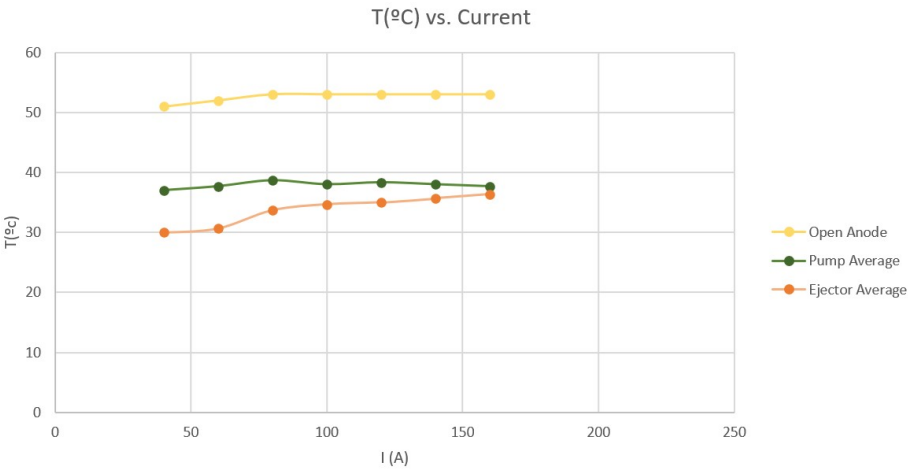

Figure 4.10: Experimental results for average inlet temperature collected for all three set-ups: OA @1.25 stoichiometry, Ejector and Pump @1.0 stoichiometry. PEMFC @65℃.

approximately a 20℃ difference between no-recirculation and recirculation operation. Finally, the fact that for the same temperature, the ejector shows less RH% than the pump RH% profile, might indicate that the ejector is not able to cope with the RH% demand of 40% at stack temperature, 65℃, at least in the range of operation of 40-160 A. In fact, according to the calculations internally performed, at 65℃ and 40% humidity, the dew point temperature, $T_{dewpoint}$, is 43.7℃. So, for the same dew point, at 35℃, the relative humidity should be 152%. This means that for the ejector set-up there's possibly a too low RH% at stack inlet since the results obtained show a RH% between 50% and 80% and not of 100% or above as for the pump.

4.1.5 Anode and Cathode Pressure Drops, $\Delta P_{Anode,Cathode}$

The pressure drop across the anode is a good indicator of the flow through the channels. Higher the flow implies higher pressure drop. Figure 4.11 presents the pressure drops difference, ΔP, measured between the anode inlet and outlet. A first analysis indicates that the pressure drop for the pump and ejector set-ups is higher than for the DQC set-up in all tests. This falls in the expected result since adding a recirculation system increases the flow rate of hydrogen across the anode although the consumed amount doesn't change. One other observation that can be withdrawn from this figure is that the pressure drop difference, ΔP, across the anode seems to be significantly variable given the fact that every single test produced unique results. This suggests that the pressure drop difference, ΔP, is a variable considerably sensitive to water droplets and sudden variations of flow rate.

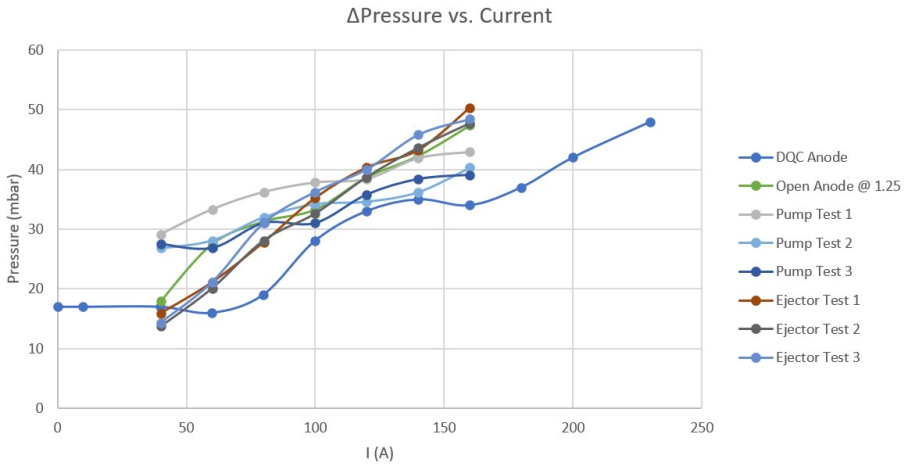

Figure 4.11: Experimental results for the anode pressure drop collected for all three set-ups: OA and DQC @1.25 stoichiometry, Ejector and Pump @1.0 stoichiometry. PEMFC @65℃.

A further analysis of the results was performed considering the average values of the anode and cathode pressure drops of all tests for both set-ups and is depicted in Figure 4.12. As expected, the cathode pressure drop stays unaltered in both situations whereas for the anode side, a significant different is observed. The fact that the pressure drop originated by the ejector set-up under 100 A is lower than the one from the pump set-up indicates that the flow recirculated is also smaller than the flow recirculated by the pump. The opposite occurs above 100 A. An analysis to the recirculated flow is elaborated in

Section 4.1.6. Figure 4.12 also indicates a maximum difference between both set-ups of approximately 10 mbar. This difference is 10% of the maximum design back-pressure of the ejector, 100 mbar.

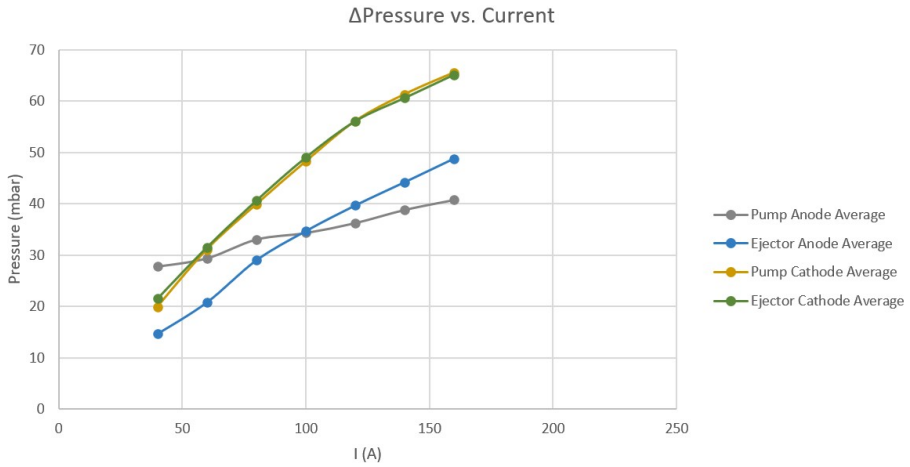

Figure 4.12: Experimental average results for the anode, @1.0 stoichiometry and cathode @2.0 stoichiometry, pressure drops collected for the ejector and Pump set-ups. PEMFC @65℃.

4.1.6 Recirculated Flow, $\dot{V}_{H_2 recirculated}$

Measuring the actual flow in the recirculation loop allows to validate the characteristics of the ejector as described in Section 3.2.3. Nevertheless, this proved not no be an easy task. Due to the fact that the stack outlet gas from the anode presents very high humidity, the flow meters available wouldn't get comprehensive readings on the anode outlet flow rate. Therefore a comparative approach was undertaken knowing that there is a relation between the pressure drop across the anode and the stoichiometry. In

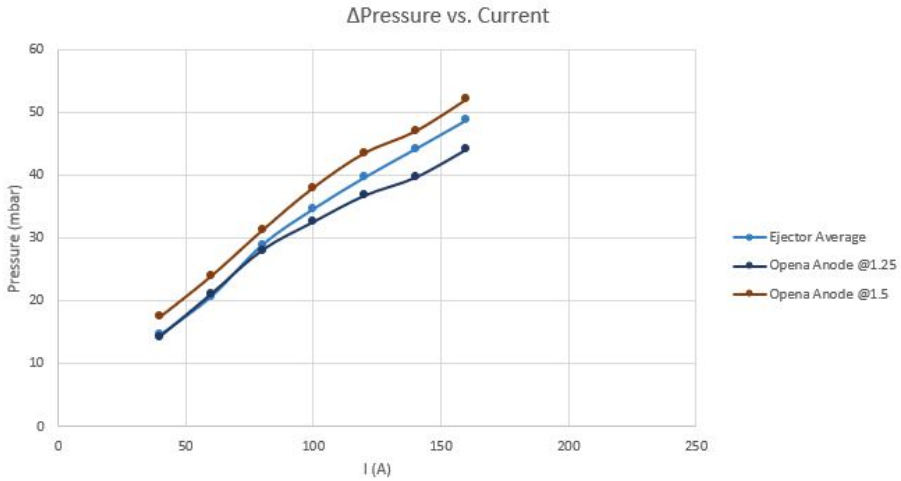

Figure 4.13: Pressure drop interpolation in the anode @1.25 stoichiometry. PEMFC @65℃.

order to have both the ejector test and the open anode at the same conditions, meaning, same dew point, the correspondent open anode temperature and humidity was calculated. For a temperature of 35ºC and 80% humidity of the inlet gas in the ejector set-up, the correspondent open anode temperature and relative humidity are 65ºC and 30%, respectively. Knowing these values, they were inserted in the

KTS and two open-anode I-V curve tests were performed for 1.25 and 1.5 stoichiometry. The results for the pressure drop measured are presented in Figure 4.13. As for the previous sections, the point at 100 A marks a transition of the behaviour of the curve. A further analysis indicates that under 100 A the stoichiometry produced by the ejector is approximately 1.25 and above 1.4. This allows to obtain the actual flow being recirculated as depicted in Figure 4.14 which shows that the ejector seems to be performing under the minimum theoretical curve. In order to better understand the results obtained, the

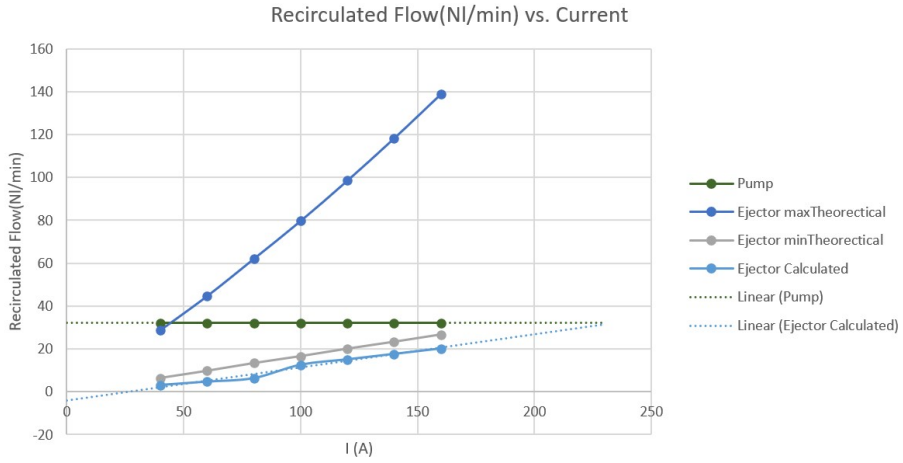

Figure 4.14: Calculated recirculation flow for the Pump and Ejector set-ups. The ejector's recirculation flow is obtained from the interpolated stoichiometry. Maximum and minimum theoretical recirculation flows of the ejector are presented. Anode stoichiometry @1.0 and PEMFC @65℃.

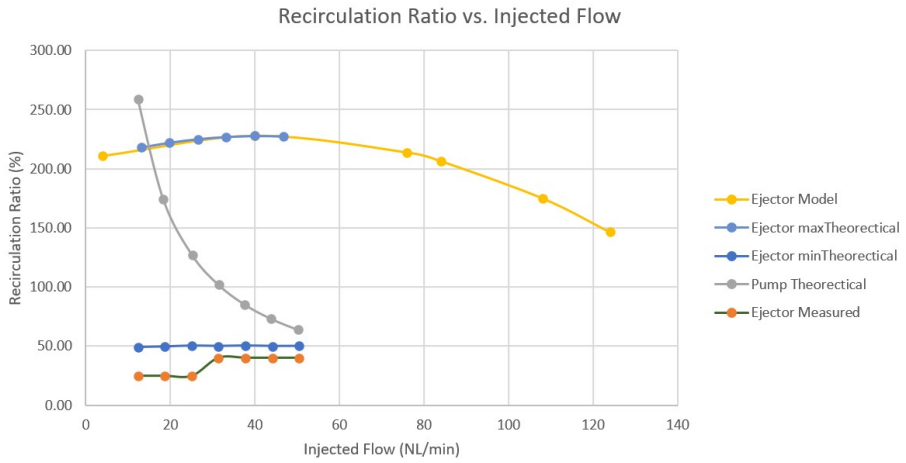

Figure 4.15: Recirculation ratio for the Pump and Ejector set-ups. The ejector recirculated flow is obtained from the interpolated stoichiometry. Maximum and minimum theoretical recirculation ratios of the ejector are presented. Anode stoichiometry @1.0 and PEMFC @65℃.

same results obtained were organized and presented in a different form in Figure 4.15, in order to match the performance graph shown in the ejector's data sheet. It clearly shows that the extracted results are approximately situated in the first half of the performance curve. In the case of the pump set-up, the curve evolves as expected from a stoichiometry of approximately 3.5 to 1.5. In the case of the ejector and as with Figure 4.14, it's visible that the ejector is performing under the minimum theoretical curve. This might be caused by multiple factors that should be studied and are presented as guidelines for

future work in Section 5.2. A main concern is that there might be too much water entering the ejector making it under perform. A reason for this suspicion is that the drain vessel did not included a filter which considerably improves the retention of water droplets. In fact upon disassemble of the ejector, a considerable amount of water was removed from the ejector's secondary inlet. Yet, another conclusion from this graphic is that the recirculation ratio might increase with current, I, as such, to perform a study on the full performance curve of the ejector might bring better understanding on it's behaviour under these conditions.

4.2 Set-ups response to start-up/shutdown and ramp-up/ramp-down procedures

4.2.1 Start-up/Shutdown

The objective of studying the behaviour of the ejector during start-up/shutdown is to verify if it is capable of dealing with a sudden no-flow to minimum flow situation and the opposite. Understanding this will allow to make changes to the procedure such as increasing the minimum flow requirement, for example. Following the start-up procedure described in Chapter 2, Hydrogen and Air flooded both the anode and cathode, respectively and the stack went into OCV. The conditions were recorded before and afterwards 40 A were drawn from the stack. The cells behaviour recorded by the Autolab software is depicted in Figure 4.16.

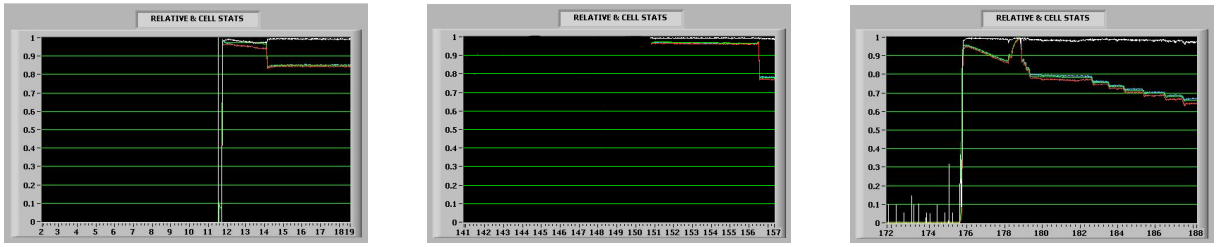

(a) Start-up with ejector (b) Start-up with pump (c) Start-up with no recirculation

Figure 4.16: Average cells voltage over time during a start-up @1.0 stoichiometry in the anode. PEMFC @65℃. Green line represents the average cells voltage. Red line represents the minimum cell voltage.

A brief observation of the three graphics indicates that the ejector does not affect the start-up of the stack/system since the reaction of the voltage in every cell is apparently almost instantaneous. The same can be observed during shutdown. After getting the stack to 40 A, the air flow in the cathode is stopped. The remaining air in the stack in consumed. This effect is observed in Figure 4.17 by the dropping voltage. Once the voltage reaches the minimum recommended value of 0.5 V per cell, the load shuts-down. At this point the stack is saturated with hydrogen and flushing is required.

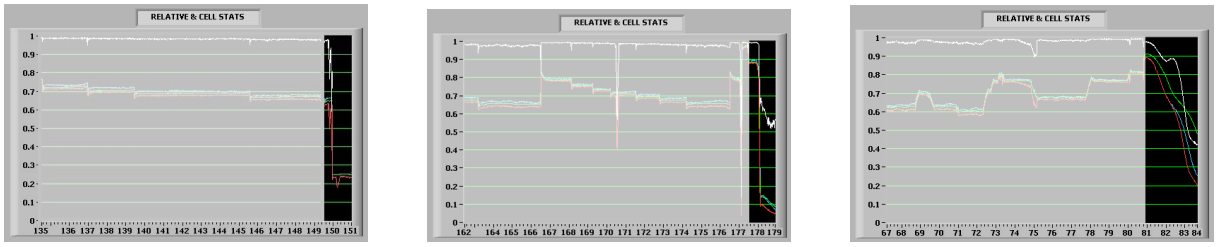

(a) Shut-down with ejector (b) Shut-down with pump (c) Shut-down with no recirculation

Figure 4.17: Average cells voltage over time during a shutdown @1.0 stoichiometry in the anode. PEMFC @65℃. Green line represents the average cells voltage. Red line represents the minimum cell voltage.

4.2.2 Ramp-up/Ramp-down

In a PEM fuel cell system application, the energy demand is expected to be instantaneous. In that regard, the components around the stack should allow an instantaneous energy production. At the anode system level, this means that the flow required for a certain energy demand should be always available. Restrictions to the flow such as too high-pressure drops are problematic. The ejector itself is a component that if not well designed or controlled can cause problems to a desired instantaneous flow demand, additionally since it is a fully mechanical device. Figure 4.18 shows a sequence of a ramp-up/ramp-down procedure for the ejector, pump and no-recirculation set-ups.

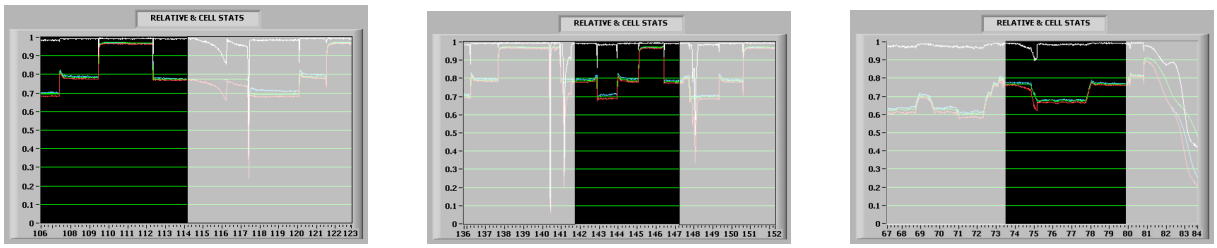

(a) Ramp-up/ramp-down sequence for the ejector (b) Ramp-up/ramp-down sequence for the pump (c) Ramp-up/ramp-down sequence with no recirculation

Figure 4.18: Average cells voltage over time during a ramp-up/ramp-down sequence @1.0 stoichiometry in the anode. PEMFC @65℃. Green line represents the average cells voltage. Red line represents the minimum cell voltage.

A brief observation of the three graphics indicates that the ejector does not affect the ramp-up of the stack/system since the reaction of the voltage in every cell is apparently almost instantaneous. The same can be observed during ramp-down. A phenomena worth mentioning is the sudden voltage drop observed at minute 80, in Figure 4.18 - (a). This sudden voltage drop was caused due to an operator error. The step at which the drop occurred was during a ramp-up from 40 A to 120 A. In order to execute this step, the operator must insert in the Autolab a value of air flow adequate to the energy production at 120 A. In this case, the load drawn energy before this value was inserted and the Autolab script had time to respond, since it operates with a small lag. Nevertheless, this observation can be considered of value since it shows that even though a voltage drop occurred, as soon as the air flow meter allowed the adequate flow of air to pass, the ejector was able by itself to also correspond with the adequate amount

of hydrogen. Figure 4.19 depicts this situation in detail.

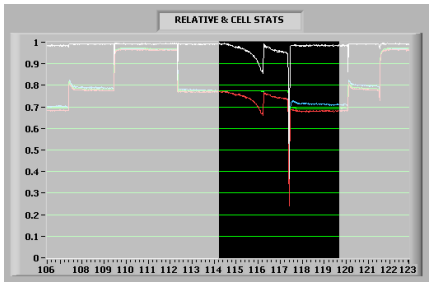

Figure 4.19: Average cell voltages over time, drop and recovery, after operator error, @1.0 stoichiometry. PEMFC @65℃. Green line represents the average cells voltage. Red line represents the minimum cell voltage.

4.3 Efficiency of pump-driven and ejector-driven recirculation

Depending on the pump at use and the size of the system where it is installed, the weight of its power consumption on the overall system efficiency varies. For this case, the pump in use was a KNF N838KNDC that consumes 45.6 W at max power.

In the case of the ejector, although the ejector itself is a mechanical device and as such does not consume energy, the peripheral system mounted around it in order to control the pressure downstream does. The HyLoop v4® at max flow has a power consumption of 18 W.

This represents a decrease of 60.5% of the energy requirement for hydrogen recirculation in the anode. Whether or not this value has relevance when compared to the overall system energy losses requires further analysis.

Chapter 5

Conclusions

5.1 Summary of contributions

The main goal of this work was to provide an insight on the use of ejectors for hydrogen recirculation in PEMFC systems. To achieve this, the use of ejectors in similar applications studied in the literature was extensively analysed. Afterwards, a product already existing in the market, HyLoop v4® was selected to fit a 5.5 kW PEM fuel cell stack and compared to KNF N838KNDC pump. Two recirculation sub-systems were designed and mounted in the test station designated for the experiments, KTS. One for the ejector and one for the pump. Normal operation and stress tests were performed in each case. The first consisted in gradually increasing the current demand in order to obtain an I-V curve. Measurements where taken in steps of 20A from 40 A to 160 A. The second one consisted in verifying the response speed and adaptability of the ejector to large current demand steps. A step of 80 A from 40 A to 120 A was studied. Both experiments had in common a Bronkhorst F-113AC-RAA-44-V flow-meter with which hydrogen flow measurements were taken. Temperature and humidity of the inlet gas mixture was obtained using Sensirion sensors. The pressure drop across the anode was measured using a GDH 13 AN GREISINGER electronic and two testo 6349 manometers. The pump set-up included a KPR1DRB412E200H0 pressure reducer and an RL4 relief valve, both from Swagelock . The important findings of this thesis are summarized and listed below:

1. Using an ejector as an alternative to pump-driven hydrogen recirculation proved to partially meet the goals stated in Section 1.6. Although the ejector proved to allow stable recirculation as well as instantaneous response to ramp-up/ramp-down procedures, it seems to fail to provide satisfactory anode humidification.
2. The hydrogen recirculation flow measured experimentally was not consistent with the stated in the product datasheet. Although it was not expected to meet the maximum recirculation profile due to the fact that hydrogen with high RH% was being used, it was expected to perform above the minimum theoretical recirculation curve. A reason for this could be the presence of water droplets in the ejector's secondary inlet.

3. The expected stoichiometry of approximately 1.0 for the main hydrogen supply was obtained when implementing recirculation allowing savings of 25% of the hydrogen used. The air stoichiometry stayed unaltered at 2.0.

4. The average deviation of the I-V curves of the ejector and the pump have an absolute average difference of 0.3V. This value is less than 1% of the lowest operating voltage registered for the OA set-up, 27.5 V.

5. The anode pressure drop originated by the pump under 100 A is higher than the one originated by the ejector and the opposite occurs above 100 A. They differ a maximum of 15 mbar which occurs at 40 A.

6. The ejector seems not to work properly below 100 A since it presents a considerably low recirculation ratio. Nevertheless it shows a tendency of increasing recirculation ration with the increase of current, I.

7. The ejector showed no signs of being affect by starting-up and shutting-down procedures as well as by 80 A interval ramp-up/ramp-down requests, demonstrating instantaneous response.

8. Replacing the pump for the venturi ejector would result in a reduction of 60% of energy savings for hydrogen recirculation in the anode.

5.2 Guidelines for future work

The work developed in this thesis led to an extensive research on ejector applications for PEMFC systems. The results obtained point to possible further research topics and improvements, guided by the current and future applications. These are listed below:

1. Submit the stack used to a DQC test would allow a full characterization of the current state of the stack while eliminating the 2% difference between the OA and DQC I-V curves.

2. Installing the ejector in a system that allows to take the same measurements and run it in the entire span of operation (up to 120 NL/min) would produce more conclusive results.

3. Understand the effects of lowering the request of 40% relative humidity at stack temperature, 65℃, for anode humidification could make the utilization of the ejector more favourable.

4. Understand the behaviour of the ejector with upstream pressure lower than 10 bar will allow to conclude whether or not the ejector could work closer to the pressure currently used in systems, 4 bar.

5. The ejector was operated at a downstream pressure of 300 mbar. Performing tests in the entire workable pressure window of the stack, 150-300 mbar allows to further characterize the ejector's performance.

Bibliography

[1] WMO. *State of the Global Climate 2020*. Number 1264:56. 2021.

[2] J. Delbeke, A. Runge-Metzger, Y. Slingenberg, and J. Werksman. The paris agreement. *Towards a Climate-Neutral Europe: Curbing the Trend*, pages 24–45, 2019.

[3] European Commission. Update of the NDC of the European Union and its Member States. (December):1–19, 2020.

[4] Hydrogen Council. Hydrogen Insights. (February):58, 2021.

[5] Global Hydrogen Review 2021. *Global Hydrogen Review 2021*, 2021.

[6] NL Netherlands. Excelling in Hydrogen: Dutch technology for a climate-neutral world. 2021.

[7] A. e. A. C. República Portuguesa and Direção Geral de Energia e Geologia. *Roteiro e plano de ação para o hidrogénio em portugal*. 2019.

[8] República Portuguesa. Estratégia Nacional-H2. 2020.

[9] Y. Liu, B. Xiao, J. Zhao, L. Fan, X. Luo, Z. Tu, and S. Hwa Chan. Performance degradation of a proton exchange membrane fuel cell with dual ejector-based recirculation. *Energy Conversion and Management: X*, 12:100114, 2021.

[10] Z. Hailun, W. Sun, H. Xue, W. Sun, L. Wang, and L. Jia. Performance analysis and prediction of ejector based hydrogen recycle system under variable proton exchange membrane fuel cell working conditions. *Applied Thermal Engineering*, 197(July):117302, 2021.

[11] K. Nikiforow, J. Pennanen, J. Ihonen, S. Uski, and P. Koski. Power ramp rate capabilities of a 5kW proton exchange membrane fuel cell system with discrete ejector control. *Journal of Power Sources*, 381(September 2017):30–37, 2018.

[12] Y. Liu, Z. Tu, and S. H. Chan. Applications of ejectors in proton exchange membrane fuel cells: A review. *Fuel Processing Technology*, 214(October 2020):106683, 2021.

[13] J. J. Hwang. Passive hydrogen recovery schemes using a vacuum ejector in a proton exchange membrane fuel cell system. *Journal of Power Sources*, 247:256–263, 2014.

[14] X. Wang, S. Xu, and C. Xing. Numerical and experimental investigation on an ejector designed for an 80kW polymer electrolyte membrane fuel cell stack. *Journal of Power Sources*, 415(October 2018):25–32, 2019.

[15] K. Nikiforow, P. Koski, and J. Ihonen. Discrete ejector control solution design, characterization, and verification in a 5 kW PEMFC system. *International Journal of Hydrogen Energy*, 42(26):16760–16772, 2017.

[16] F. Li, J. Du, L. Zhang, J. Li, G. Li, G. Zhu, M. Ouyang, J. Chai, and H. Li. Experimental determination of the water vapor effect on subsonic ejector for proton exchange membrane fuel cell (PEMFC). *International Journal of Hydrogen Energy*, 42(50):29966–29970, 2017.

[17] M. L. Ferrari, M. Pascenti, and A. F. Massardo. Validated ejector model for hybrid system applications. *Energy*, 162:1106–1114, 2018.

[18] B. M. Tashtoush, M. A. Al-Nimr, and M. A. Khasawneh. A comprehensive review of ejector design, performance, and applications. *Applied Energy*, 240(January):138–172, 2019.

[19] F. Barbir. *PEM Fuel Cells: Theory and Practice*. Academic Press, 2nd edition, 2012.

[20] R. K. Ahluwalia and X. Wang. Fuel cell systems for transportation: Status and trends. *Journal of Power Sources*, 177(1):167–176, feb 2008.

[21] J. Cooper, S. Grot, and C. Hartnig. 5 - recycling and life cycle assessment of fuel cell materials. In C. Hartnig and C. Roth, editors, *Polymer Electrolyte Membrane and Direct Methanol Fuel Cell Technology*, volume 1 of *Woodhead Publishing Series in Energy*, pages 117–134. Woodhead Publishing, 2012.

[22] H. Chen, Z. Song, X. Zhao, T. Zhang, P. Pei, and C. Liang. A review of durability test protocols of the proton exchange membrane fuel cells for vehicle. *Applied Energy*, 224:289–299, 2018.

[23] Y. Song, X. Wang, L. Wang, F. Pan, W. Chen, and F. Xi. A twin-nozzle ejector for hydrogen recirculation in wide power operation of polymer electrolyte membrane fuel cell system. *Applied Energy*, 300(July):117442, 2021.

[24] J. G. Hayes and G. A. Goodarzi. *Electric powertrain: Energy systems, power electronics & drives for hybrid, electric & fuel cell vehicles*. 2019.

[25] W. B.D.B.Gou. *Fuel Cells: Dynamic Modeling and Control with Power Electronics Applications*, volume 44. 2017.

[26] M. Arif, S. C. Cheung, and J. Andrews. A systematic approach for matching simulated and experimental polarization curves for a PEM fuel cell. *International Journal of Hydrogen Energy*, 45: 2206–2223, 1 2019.

[27] S. Toghyani, E. Afshari, and E. Baniasadi. A parametric comparison of three fuel recirculation system in the closed loop fuel supply system of PEM fuel cell. *International Journal of Hydrogen Energy*, 44(14):7518–7530, 2019.

[28] W. Wiebe, T. v. Unwerth, and S. Schmitz. Using of an Electrochemical Compressor for Hydrogen Recirculation in Fuel Cell Vehicles. *Fuel Cells*, 20(3):362–369, 2020.

[29] S. Rodosik, J. P. Poirot-Crouvezier, and Y. Bultel. Impact of humidification by cathode exhaust gases recirculation on a PEMFC system for automotive applications. *International Journal of Hydrogen Energy*, 44(25):12802–12817, 2019.

[30] S. Erbach, B. Pribyl, M. Klages, L. Spitthoff, K. Borah, S. Epple, L. Gubler, P. Alexandra, M. Heinen, and T. J. Schmidt. ScienceDirect Influence of operating conditions on permeation of CO 2 through the membrane in an automotive PEMFC system. pages 1–12, 2018.

[31] P. Koski, J. Viitakangas, and J. Ihonen. Determination of fuel utilisation and recirculated gas composition in dead-ended PEMFC systems. *International Journal of Hydrogen Energy*, 45(43):23201–23226, 2020.

[32] J. Hou, M. Yang, and J. Zhang. Active and passive fuel recirculation for solid oxide and proton exchange membrane fuel cells. *Renewable Energy*, 155:1355–1371, 2020.

[33] P. Pei, M. Ouyang, W. Feng, L. Lu, H. Huang, and J. Zhang. Hydrogen pressure drop characteristics in a fuel cell stack. 31:371–377, 2006.

[34] J. Hwang, D. Wang, and N. Shih. Development of a lightweight fuel cell vehicle. *Journal of Power Sources*, 141(1):108–115, 2005.

[35] M. Badami and M. Mura. Theoretical model with experimental validation of a regenerative blower for hydrogen recirculation in a PEM fuel cell system. *Energy Conversion and Management*, 51(3): 553–560, 2010.

[36] Z. Liu, Z. Liu, K. Jiao, Z. Yang, X. Zhou, and Q. Du. Numerical investigation of ejector transient characteristics for a 130-kW PEMFC system. *International Journal of Energy Research*, 44(5): 3697–3710, 2020.

[37] Y. Zhu, W. Cai, Y. Li, and C. Wen. Anode gas recirculation behavior of a fuel ejector in hybrid solid oxide fuel cell systems: Performance evaluation in three operational modes. *Journal of Power Sources*, 185(2):1122–1130, 2008. ISSN 03787753.

[38] A. V. K. B. K. McCurdy. Development of PEMFC systems for space power applications. pages 1–7, 2003.

[39] P. H. Huang, J. K. Kuo, W. Z. Jiang, and C. B. Wu. Simulation analysis of hydrogen recirculation rates of fuel cells and the efficiency of combined heat and power. *International Journal of Hydrogen Energy*, 46(31):16823–16835, 2021.

[40] J. K. Kuo, W. Z. Jiang, C. H. Li, and T. H. Hsu. Numerical investigation into hydrogen supply stability and I-V performance of PEM fuel cell system with passive Venturi ejector. *Applied Thermal Engineering*, 169:114908, 2020.

[41] D. Jenssen, O. Berger, and U. Krewer. Improved PEM fuel cell system operation with cascaded stack and ejector-based recirculation. *Applied Energy*, 195:324–333, 2017.

[42] N. fuel cell technology B.V. . Installation and Operation Manual Nedstack PEM Fuel Cell Stack. 2010.

Appendix A

Version: February 2014

NEDSTACK FCS 5-HP
PEM FUEL CELL STACK

SPECIFICATIONS

Electrical - Beginning of Life

Power maximum	:	5 kWe @ 230 A
Power at lower current	:	see Table 1

Mechanical

Weight	:	28 kg (approx)
Size	:	353(l)x194(w)x288(h) mm
Cell count	:	40

Hydrogen

Humidification	:	≥ 40% RH at 65 ºC at inlet
Purity (dry)	:	Grade ≥ 2.5 (max: CO 0.2ppm, CO2 0.5vol%, total sulphur 4ppb, formaldehyde 0.01ppm, formic acid 0.2ppm, ammonia 0.1ppm, total halogenated compounds 0.05ppm, particles 1µg/Nl. Hydrogen specification adapted from ISO 14687-2:2008)
Pressure drop	:	< 0.05 bar at full power
Pressure level	:	0.15 - 0.3 barg
Stoichiometry	:	1.25 - 1.50 for H_2 , minimum flow = 24 Nl/min
Max H2 consumption	:	64 Nl/min at full power

Air

Filtered

Humidification	:	≥ 40% RH at 65 ºC
Purity	:	instrument air quality (max: CO 25ppm, Sulphur 0.01ppm, nitrogen dioxide 0.3ppm, ammonia 1ppm, particles 1µg/Nl)
Pressure level	:	Ambient (no backpressure allowed)
Pressure drop	:	< 0.12 bar at max power
Stoichiometry	:	≥ 2.0
Max air required	:	305 Nl/min at full power

MEA

Pressure difference		<0.3 bar

Emissions

Noise	:	0
Water	:	3.1 kg/hour (approx.)
H2	:	25 ml/min (max)

Nedstack
PEM FUEL CELLS

Cooling

Nominal temperature	:	65 °C
$Temperature_{max}$	:	≤ 70 °C
Capacity	:	< 8.3 kW_{th} at full power
Medium	:	de-mineralized water or BASF glysantine FC G20
Purity	:	conductivity < 10 µS.cm^{-1}
Pressure difference	:	< 0.15 bar (DI water) or < 0.45 bar for glysantine
Operating window	:	ΔT < 5K

Note that proper material selection in the tempering device is important to avoid release of ions into the coolant

Connectors

Coolant	*standard*	:	Nedstack quick coupling (male)
	optional	:	¾ inch HAM-let/Swagelok compatible or Nedstack quick coupling (female)
Hydrogen	*standard*	:	Nedstack quick coupling (male)
	optional	:	¾ inch HAM-let/Swagelok compatible or Nedstack quick coupling (female)
Air	*standard*	:	Nedstack quick coupling (male)
	optional	:	32 mm OD, hose clamp connection or Nedstack quick coupling (female)
Current		:	End contact with 8 mm hole
Cell voltage connector		:	1 DD50 female connector

Stack Connection lay-out:

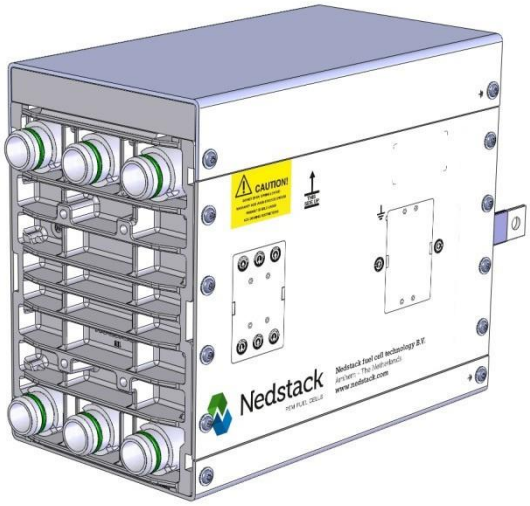

Nedstack
fuel cell technology B.V.

Westervoortsedijk 73
6827 AV ARNHEM

P.O. Box 5167
6802 ED ARNHEM
The Netherlands

Phone +31 (0)26 319 7600
Fax +31 (0)26 319 7601
E-mail info@nedstack.com

Trade Register Arnhem
nr. 09102161

www.nedstack.com

Nedstack
PEM FUEL CELLS

Electrical specifications

Minimum Beginning of Life stack performance data under standard conditions*

Current (A)	0	10	40	80	120	150	180	200	230
Stack V (V)	38.7	34.3	31.6	29.3	27.5	26.2	24.8	23.8	22.1
Stack P (kW)	0	0.34	1.26	2.34	3.30	3.93	4.46	4.75	5.09
Cell V (mV)	967	857	789	732	687	655	620	594	553

*standard conditions:
Stack temperature = 62 °C,
Hydrogen: stoichiometry = 1.25; minimum hydrogen flow = 24 Nl/min; RH = 80%.
Air: stoichiometry = 2.0; minimum air flow = 56 Nl/min; RH = 80%

Nedstack
fuel cell technology B.V.

Westervoortsedijk 73
6827 AV ARNHEM

P.O. Box 5167
6802 ED ARNHEM
The Netherlands

Phone +31 (0)26 319 7600
Fax +31 (0)26 319 7601
E-mail info@nedstack.com

Trade Register Arnhem
nr. 09102161

www.nedstack.com

Appendix B

N 838 SERIES
VACUUM PUMPS

N 838 KNDC

ADVANTAGES

- Excellent price/performance ratio
- High level of performance in a compact size

POSSIBLE AREAS OF USE

- Instrumental analysis (i.a. degassing)
- Diagnostics – disposal of sample waste
- Vacuum technology – pick & place applications
- Medical technology – OR-suction devices

Please visit our website
www.knf.com
to get more information

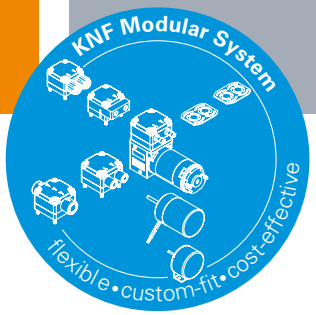

PERFORMANCE DATA						
Series model	**N 838**					
Material design	**KNE**	**ANE**	**KNDC**	**ANDC**	**KNDC-B**	**KN.29 DC-B**
Pump head	PPS	Aluminum	PPS	Aluminum	PPS	
Diaphragm	EPDM					
Valves	FPM					
Flow rate at atm. pressure (l/min)	34.0		32.0		34.0	8.5–34.0
Ultimate vacuum (mbar abs.)	100					
Max. operating pressure (bar rel./psig)	0.5/7.3					
Permissible ambient temperature (°C)	+5 ... +40					
Permissible media temperature (°C)	+5 ... +40					
Weight (kg/lbs)	2.3/5.1		2.2/4.8	2.4/5.3	2.0/4.4	
ELECTRICAL DATA						
Voltage (V)	230		12 | 24		24	
Motor	Capacitor motor		DC motor		Brushless DC motor	
Protection class motor	IP 00		IP 50		IP 20	
Frequency (Hz)	50		-			
Power P_1 (W)	100.0		-		58.0	
I_{max} (A)	0.60		3.7 | 1.9		2.40	

N 838 KNE | ANE

PERFORMANCE DATA

Series model	Flow rate at atm. pressure (l/min)[1)]	Max. operating pressure (bar rel./psig)	Ultimate vacuum (mbar abs.)
N 838 KNE	34.0	0.5/7.3	100
N 838 ANE	34.0	0.5/7.3	100

[1)] Liter at STP

N 838 _NE

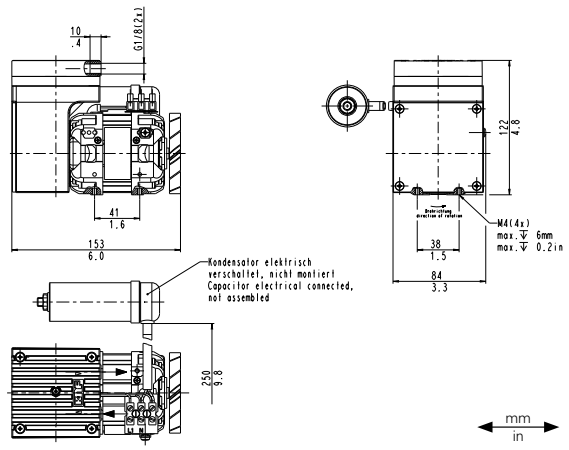

N 838 _NE

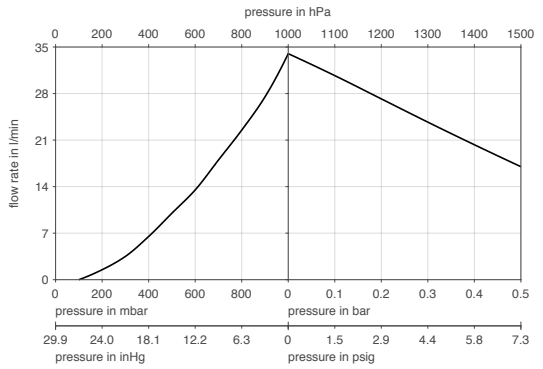

N 838 _NE | PUMP DOWN TIME FOR 10 LITER VESSEL

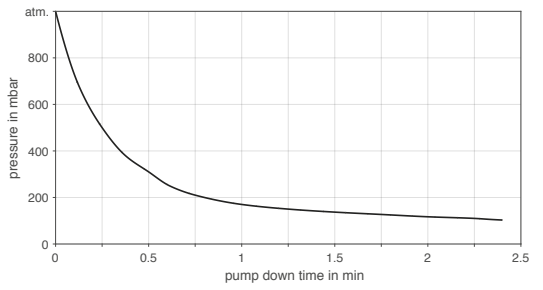

N 838 KNDC | ANDC | KNDC-B | KN.29 DC-B

PERFORMANCE DATA

Series model	Flow rate at atm. pressure (l/min)[1]	Max. operating pressure (bar rel./psig)	Ultimate vacuum (mbar abs.)
N 838 KNDC	32.0	0.5/7.3	100
N 838 ANDC	32.0	0.5/7.3	100
N 838 KNDC-B	34.0	0.5/7.3	100
N 838 KN.29 DC-B	8.5–34.0	0.5/7.3	100

[1] Liter at STP

N 838 _NDC

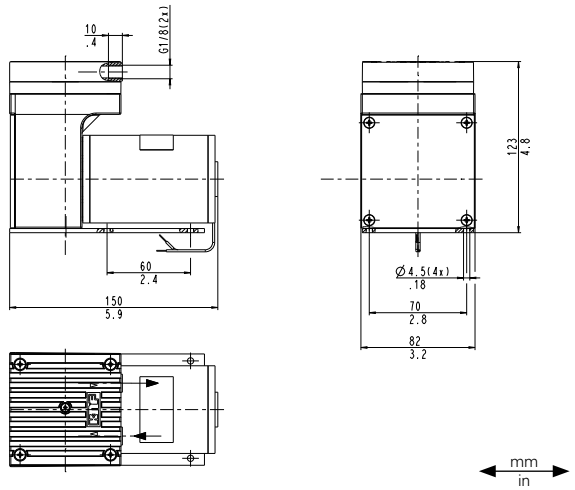

N 838 KNDC-B | KN.29 DC-B

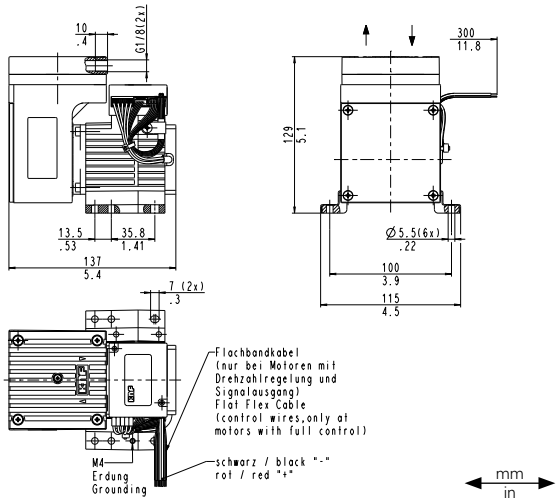

N 838 _NDC

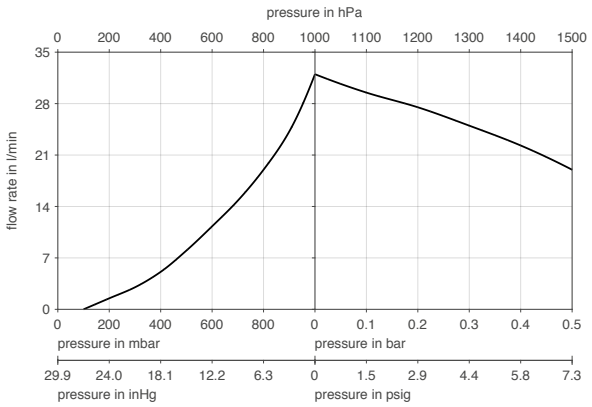

N 838 KNDC-B

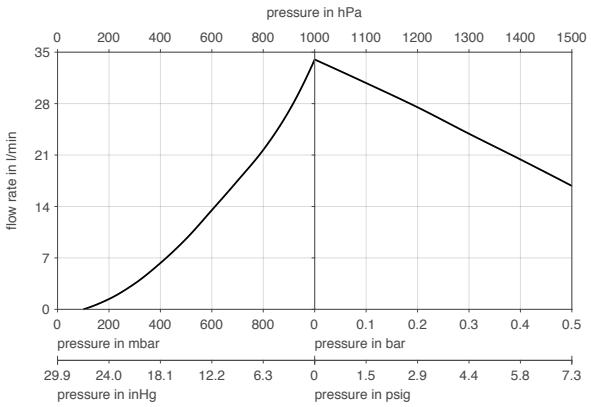

N 838 KN.29 DC-B

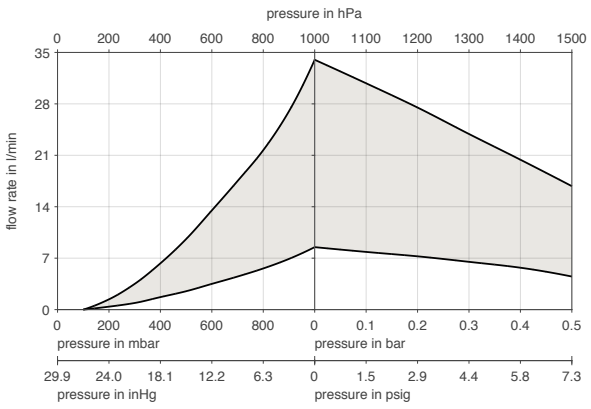

ACCESSORIES

Description	Part No.	Details
Silencer/Inlet filter	007006	G 1/8
Hose connector	000360	G 1/8 PA

SPARE PARTS

Description	Part No.	Details
Spare parts kit	043825	

The performance values for the series models shown on this data sheet were determined under test conditions.
The actual performance values may differ and depend in particular on the usage conditions and therefore on the specific application, on the parameters of the components involved in the user's system and on any technical modifications carried out which deviate from the standard configuration or the as delivered condition.

If individual designs have been created for specific customers on the basis of series models, other technical performance data may apply.
Before operation begins, the relevant operating instructions and/or assembly or installation instructions should be read and the safety information contained in these instructions should be noted.
KNF reserves the right to make changes to the product and the associated documentation without prior notice to the customer.

www.knf.com

Appendix C

AD-VENTA
INNOVATIVE

Hydrogen Recirculation/Regulation System
Product datasheet

HyLoop® is an Hydrogen recirculation system for fuel cell.
HyLoop® also provides the pressure regulation of the hydrogen flow.
The mechanism and the electronical design are the result of **Ad-Venta**'s expertise.
Ad-venta offers a dedicated technical support for the integration of this product with the corresponding fuel cell.

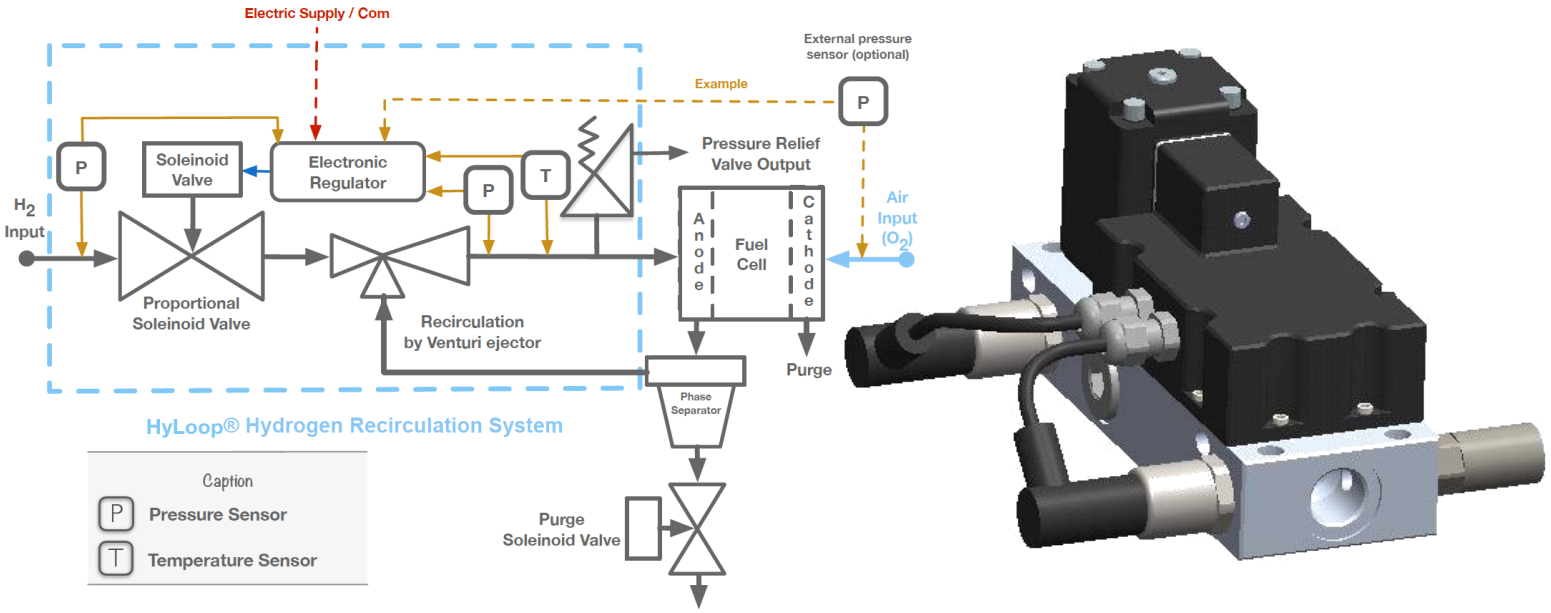

HyLoop v4® - Mechanical Specifications

Dimensions	196 mm x 180 mm x 106 mm (Single) 196 mm x 235 mm x 106 mm (Dual)	
Weight	2.1 kg (Single) – 3,8 kg (Dual)	
External materials	Bloc : Aluminum (Anodized) Casing : ABS	
Internal materials	Aluminium (Anodized) Stainless steel (316L)	
Fluid recommendations	Inlet : **Hydrogen** Recirculation : Nitrogen, Hydrogen, Water Vapor (and **all outlet gas from a Fuel Cell**)	
Fluid temperature	Inlet: -10°C / +90°C Recirculation: -10°C / +90°C	
Ambiant temperature	-20°C / +55°C	
Max emitted temperature	+ 80°C	
Inlet working pressure	**10 barg** (+/- 0.5 barg)	
Inlet max pressure	**12.5 barg**	
Outlet pressure	Adjustable from **0.1 to 2 barg**	
Inlet flow rate (H_2)	From 5 to 1300 NLPM (5 flow ranges) ➔ **1.5 kW to 100 kW** Fuel Cell	
Recirculation ratio (H_2)	Higher than **50%** of the inlet flow (for each range of power)	
Connections	BSPP female ports: Inlet : G1/4" Recirculation : G1/2" Outlet : G1/2" Safety valve **(option)**: G3/8"	Inlet/Outlet fittings on demand: - Stainlees steal tube fitting - Quick coupling flexible - Barb

HyLoop v4® - Dimensional drawings

- HyLoop 5 – 50 kW

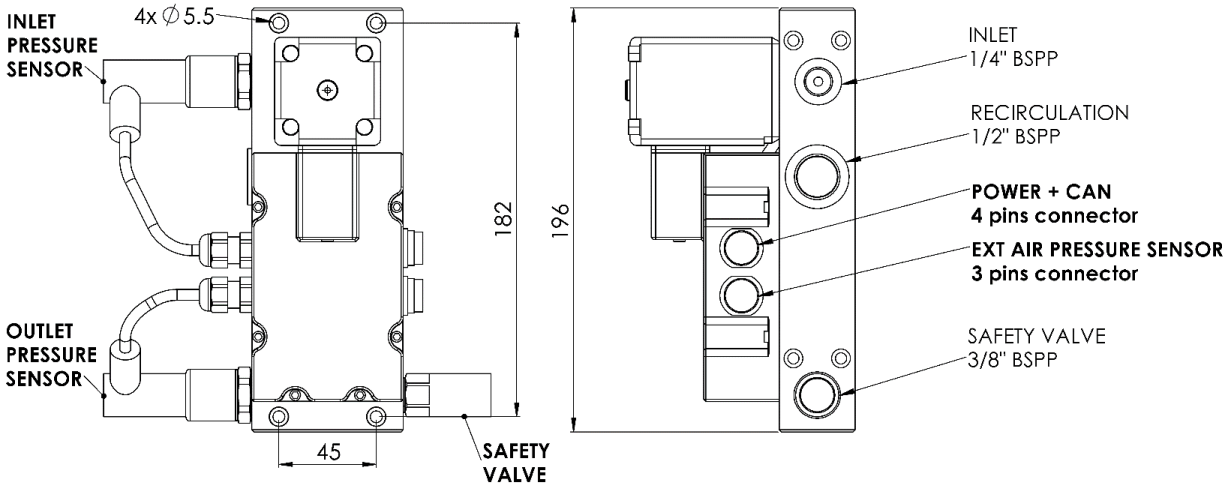

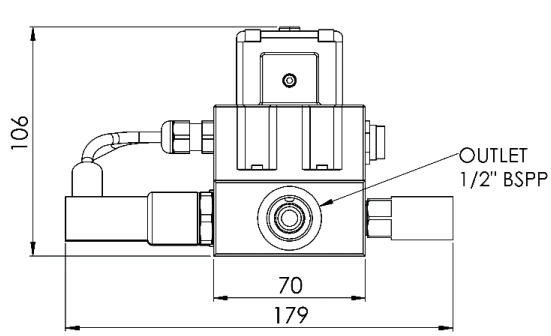

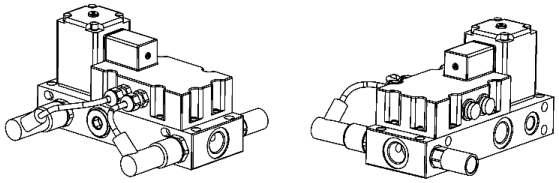

- HyLoop 100kW

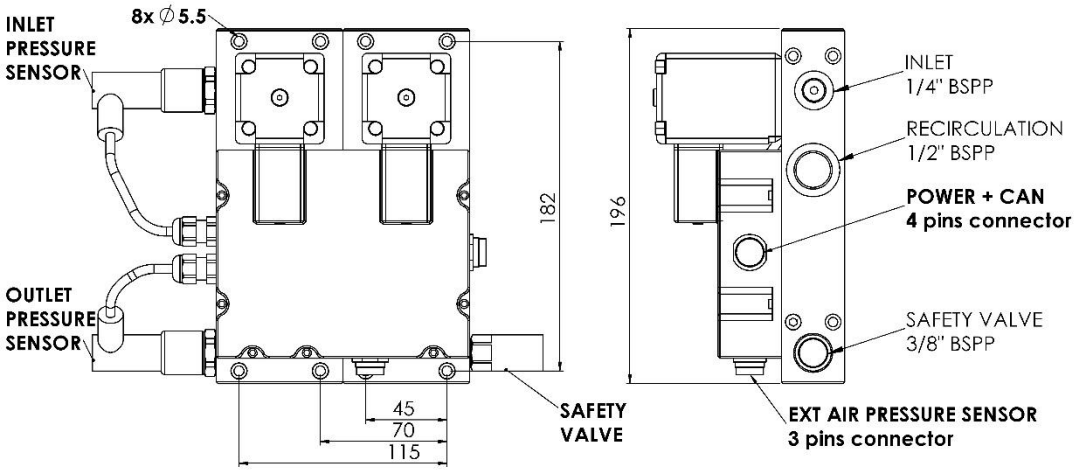

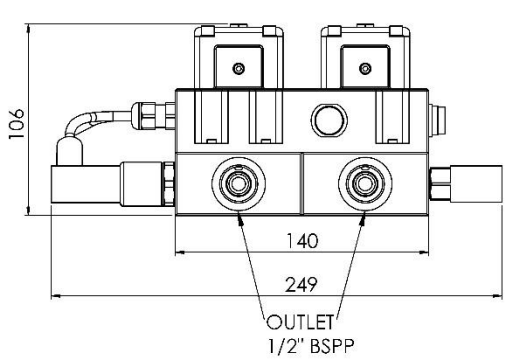

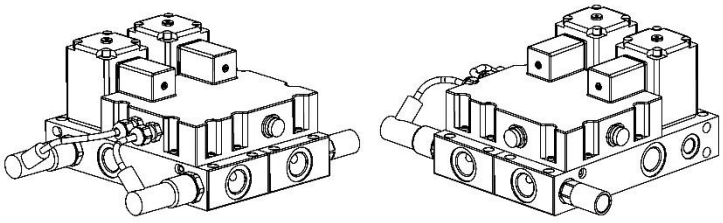

AD-VENTA
INNOVATIVE

HyLoop v4® - Components and accessories

Electrical supply	**12V** DC or **24V** DC (on demand)
Power consumption	1 W (at rest) – 18W (max flow)
Electrical connectors	Cliffcon® - IP 68 **4 pins** (CAN and power supply) **3 pins** (external sensor)
Communication protocol	CAN

4 pins conector		
	1	Alim +
	2	Alim -
	3	CanH
	4	CanL

3 pins conector		
	1	Alim +
	2	Alim -
	3	Signal

	Pressure sensors		
Type	**Inlet**	**Outlet**	**Air pressure** (optional ext sensor)
Measuring range	0 – 16 barg	0 – 2.5 barg	0 – 2.5 barg
Max allowable pressure	40 barg	7.5 barg	7.5 barg
Accuracy	+/- 48 mbar	+/- 7.5 mbar	+/- 7.5 mbar
Other (adjustable on demand)	X	X	Cable length: On demand Connexion: G 1/8'' or G 1/4 ''

	Power/data cable
Length	3m (adjustable on demand)
HyLoop side	4 pins connector
Client side	Banana plug (power) 2x 22AWG wires

	Safety valve (option)
Type	Mini VentHy – Ad-Venta
Pressure setting	Factory set from 0.3 to 14 barg
Outlet connexion	Without quick fitting: G 3/8" (BSPP) Female Fitting on demand (min 7mm internal diameter)

HyLoop® v4 - Control

HyLoop® v4 is controlled by CAN protocol.
There are 2 main piloting modes:

- "Pressure": CAN master provides a pressure value that the regulator will maintain at HyLoop® outlet.
- "Pressure Delta": CAN master provides a pressure delta value that the regulator will maintain between the external air pressure sensor and HyLoop® outlet.

Details on "HyLoop v4 user guide" and "DBC register file".

HyLoop® v4 - Model list and references

HyLoop®		
Fuel cell power	**Supply voltage**	**Reference**
1.5 kW	12 V	AH_010_01
	24 V	AH_011_01
5 kW	12 V	AH_020_01
	24 V	AH_021_01
20 kW	12 V	AH_030_01
	24 V	AH_031_01
50 kW	12 V	AH_040_01
	24 V	AH_041_01
100 kW	12 V	AH_050_01
	24 V	AH_051_01

Options		
Component	**Specification**	**Reference**
External air sensor	G 1/8'' BSPP	S1_196_01
	G 1/4'' BSPP	S1_206_01
MiniVentHy safety valve	On demand	On demand
Accessories		
Component	**Specification**	**Reference**
Cable (included)	Power + data	J4_111_01

Recirculation effiency curves

Gas : 100% H2, dry (main flow and recirculated flow). Tests conducted on Ad-Venta test bench.

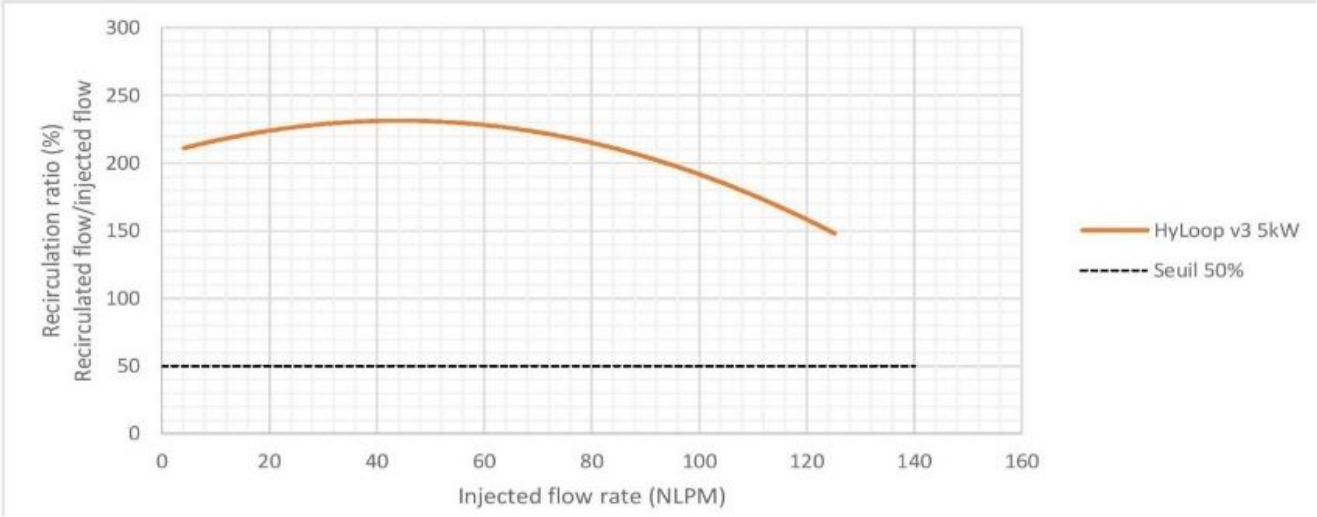

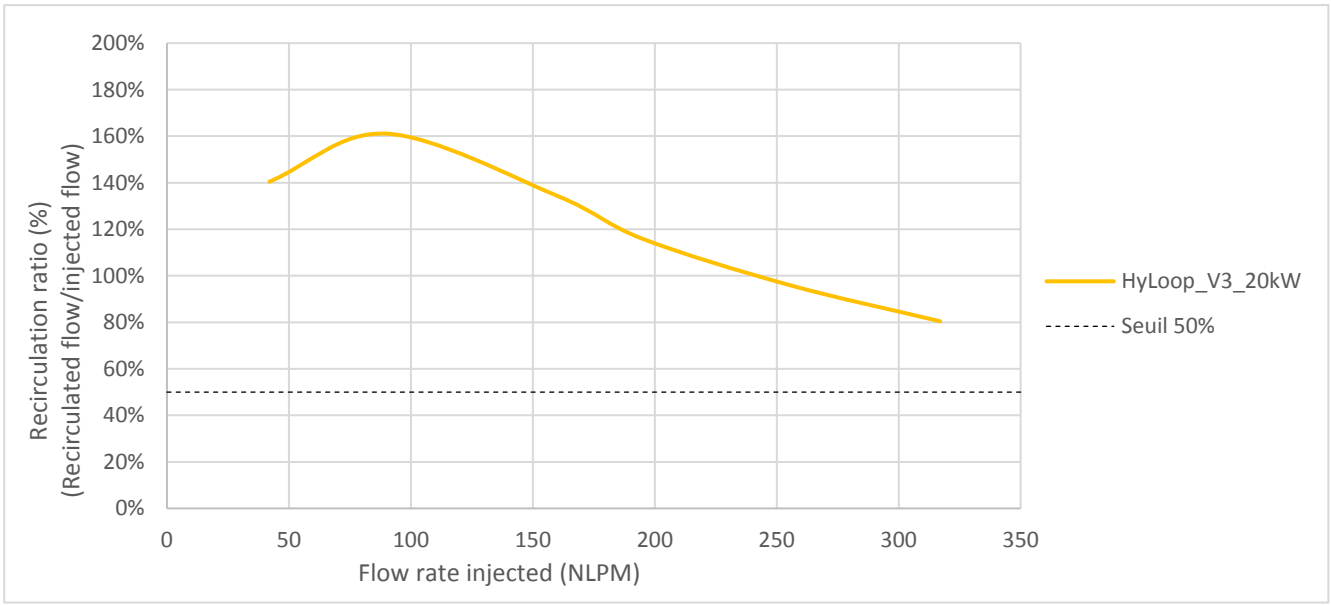

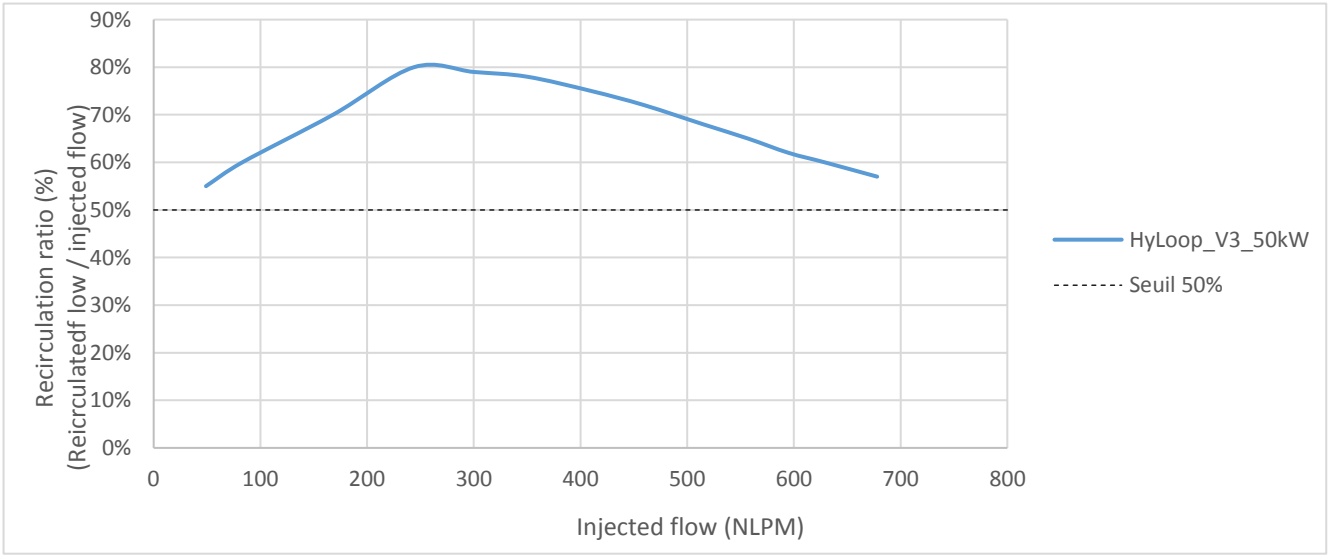

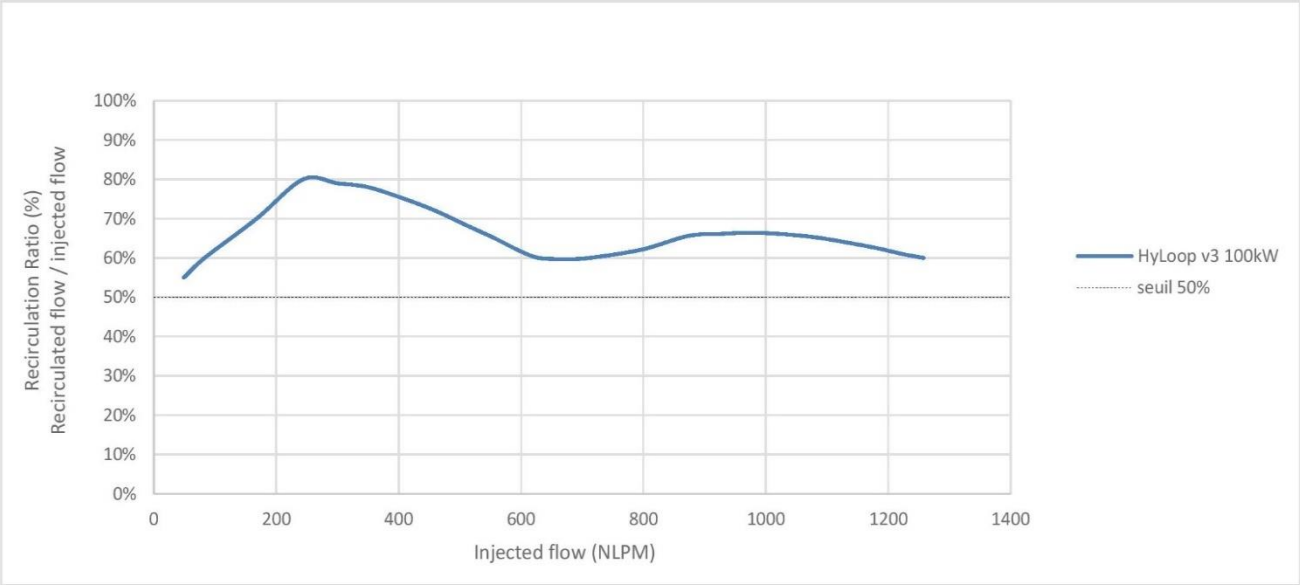
Recirculation Ratio (%)
Recirculated flow / injected flow
100%
90%
80%
70%
60%
50%
40%
30%
20%
10%
0%
0
200
400
600
800
1000
1200
1400
Injected flow (NLPM)
HyLoop v3 100kW
seuil 50%

Appendix D

Nedstack PEM FUEL CELLS	Experiment Form	KTS

Set-Up:

Created by: PR

Basic Performance Test:

I (A)	U (V)	Tstack in (ºC)	Tstack out (ºC)	Anode ΔP(mbar)	Cathode ΔP(mbar)	Anode T(ºC) in/out	Anode RH% in/out	Flow A/C (slpm)	Stoich A/C
0						/	/	/	/
40						/	/	/	/
60						/	/	/	/
80						/	/	/	/
100						/	/	/	/
120						/	/	/	/
140						/	/	/	/
160						/	/	/	/

Stress Test:

	I (A)	U (V)	Tstack in (ºC)	Tstack out (ºC)	Anode ΔP(mbar)	Cathode ΔP(mbar)	Anode T(ºC) in/out	Anode RH% in/out	Flow A/C (slpm)	Stoich A/C	tts (s)
Start-up	0						/	/	/	/	
	40						/	/	/	/	
Ramp-up	40						/	/	/	/	
	120						/	/	/	/	
Ramp-down	120						/	/	/	/	
	40						/	/	/	/	
Shut-down	40						/	/	/	/	
	0						/	/	/	/	

Comments: